Inhibition of Cdk6 Expression Through p38 MAP Kinase Is Involved in Differentiation of Mouse Prechondrocyte ATDC5

TORU MORO,[1] TORU OGASAWARA,[1] HIROTAKA CHIKUDA,[1] TOSHIYUKI IKEDA,[1] NAOSHI OGATA,[1] ZENJIRO MARUYAMA,[2] TOSHIHISA KOMORI,[2] KAZUTO HOSHI,[1] UNG-IL CHUNG,[1] KOZO NAKAMURA,[2] HIROTO OKAYAMA,[3] AND HIROSHI KAWAGUCHI[1]*

[1]*Department of Sensory and Motor System Medicine, Faculty of Medicine, University of Tokyo, Tokyo, Japan*

[2]*Division of Oral Cytology and Cell Biology, Nagasaki University Graduate School of Biomedical Sciences, Nagasaki, Japan*

[3]*Department of Biochemistry and Molecular Biology, Faculty of Medicine, University of Tokyo, Tokyo, Japan*

Because a temporal arrest in the G1-phase of the cell cycle is a prerequisite for cell differentiation, this study investigated the involvement of cell cycle factors in the differentiation of cultured mouse prechondrocyte cell line ATDC5. Among the G1 cell cycle factors examined, both protein and mRNA levels of cyclin-dependent kinase (Cdk6) were downregulated during the culture in a differentiation medium. The protein degradation of Cdk6 was not involved in this downregulation because proteasome inhibitors did not reverse the protein level. When inhibitors of p38 MAPK, ERK-1/2, and PI3K/Akt were added to the culture, only a p38 MAPK inhibitor SB203580 blocked the decrease in the Cdk6 protein level by the differentiation medium, indicating that the Cdk6 inhibition was mediated by p38 MAPK pathway. In fact, p38 MAPK was confirmed to be phosphorylated during differentiation of ATDC5 cells. Enforced expression of Cdk6 in ATDC5 cells blocked the chondrocyte differentiation and inhibited Sox5 and Sox6 expressions. However, the Cdk6 overexpression did not affect the proliferation or the cell cycle progression, suggesting that the inhibitory effect of Cdk6 on the differentiation was exerted by a mechanism largely independent of its cell cycle regulation. These results indicate that Cdk6 may be a regulator of chondrocyte differentiation and that its p38-mediated downregulation is involved in the efficient differentiation. J. Cell. Physiol. 204: 927–933, 2005. © 2005 Wiley-Liss, Inc.

Endochondral ossification is an essential process for embryonic development, skeletal growth, and fracture healing. This highly regulated process involves the coordination of chondrocyte proliferation and differentiation to give rise to the cartilaginous structures, which are subsequently replaced by bone (Karsenty and Wagner, 2002). Chondrocytes that are derived from mesenchymal cells proliferate to expand the cartilage mold, and then form columns of flattened proliferative cells. Chondrocytes then permanently exit the cell cycle, and postmitotic cells further differentiate into prehypertrophic and hypertrophic chondrocytes, which secrete an extracellular matrix that becomes mineralized. Analyses of transgenic and knockout mice have demonstrated that disturbance of the fine balance between chondrocyte proliferation and differentiation can cause skeletal defects such as skeletal dysplasias (Mundlos and Olsen, 1997a,b; Serra et al., 1997). Thus, in this process of endochondral bone formation, proliferation and differentiation of chondrocytes must be properly coordinated; however, the molecular processes regulating these functions remain largely unknown.

Cell cycle factors appear to play an important role in the control of chondrocyte proliferation and differentiation (Beier et al., 1999a; LuValle and Beier, 2000). Proliferation of eukaryotic cells depends on their progression through the cell cycle, and at least a temporal cell cycle arrest at the G1-phase is thought to be a prerequisite for cell differentiation (Sherr, 1994). Complexes of cyclin and cyclin-dependent kinase (Cdk) promote G1/S-phase transition by phosphorylating the retinoblastoma (Rb) pocket protein family members Rb, p107, and p130. Phosphorylation of the pocket protein blocks their ability to repress E2F family members, leading to activation of genes required for S-phase entry. The predominant G1 cyclin–Cdk complexes are cyclin D-Cdk4/6, and in late G1, cyclin E-Cdk2. The D-type cyclins are upregulated by mitogenic stimuli (Coqueret, 2002), and cyclin–Cdk complexes are inhibited by two major families of Cdk inhibitors (CKIs) (Sherr and Roberts, 1999). The INK4 family specifically binds and inactivates monomeric Cdk4 or Cdk6, whereas the CiP/KiP family, which includes p21, p27, and p57, inhibits all G1/S-phase cyclin–Cdk complexes, except for the cyclin D3–Cdk6 complex (Lin et al., 2001).

Since in lower eukaryotes the control of cell cycle factors driving S-phase onset greatly influences the commitment to cell differentiation, the present study investigated the possibility of crucial participation of these factors in chondrocyte differentiation using a mouse prechondrocyte cell line ATDC5, and found that in the differentiation medium containing insulin Cdk6 was downregulated primarily by p38 mitogen-activated protein kinase (MAPK) signal-invoked transcriptional

Contract grant sponsor: Japanese Ministry of Education, Culture, Sports, Science, and Technology; Contract grant numbers: 14657358, 16659402.

*Correspondence to: Hiroshi Kawaguchi, Department of Sensory and Motor System Medicine, Faculty of Medicine, University of Tokyo, Hongo 7-3-1, Bunkyo, Tokyo 113-8655, Japan.
E-mail: kawaguchi-ort@h.u-tokyo.ac.jp

Received 10 September 2004; Accepted 7 January 2005

Published online in Wiley InterScience (www.interscience.wiley.com.), 28 March 2005.
DOI: 10.1002/jcp.20350

repression and that its down-regulation was involved in the efficient differentiation.

MATERIALS AND METHODS

Reagents and antibodies

Insulin-transferrin-sodium selenite supplement (ITS) was purchased from Roche Molecular Biochemicals (Mannheim, Germany). Antibodies against Cdk2 (H-298), Cdk4 (C-22), Cdk6 (C-21), cyclin A (C-19), cyclin D1 (C-20), cyclin D2 (M-20), cyclin D3 (C-16), cyclin E (M-20), p15 (K-18), p16 (H-156), p18 (M-20), p19 (M-20), p21 (M-19), p27 (F-8), and p57 (C-20) were obtained from Santa Cruz Biotechnology (Santa Cruz, CA). Antibodies against p38 MAPK (#9212) and phosphorylated p38 MAPK (#9211S) were purchased from Cell Signaling Technology, Inc. (Beverly, MA). Antibodies against β-actin (AC-15) were purchased from Sigma Chemical Co. (St. Louis, MO). 4-(4-fluorophenyl)-2-(4-methylsulfinylphenyl)-5-(4-pyridyl)-1H-imidazole (SB203580), 2-(4-morpholinyl)-8-phenyl-4H-1-benzopyran-4-one (LY294002), and 2′-Amino-3′-methoxyflanone (PD98059) were purchased from Calbiochem Novabiochem Co. (La Jolla, CA).

Cell culture

Mouse prechondrocyte cell line ATDC5 cells were purchased from the Riken Cell Bank (Tsukuba, Japan). The cells were maintained in Dulbecco's minimal essential medium nutrient mixture F-12 HAM (DMEM/F12; Sigma) containing 5% fetal bovine serum (FBS; Sigma) in 5% CO_2 in air. For induction of chondrogenesis, cells were inoculated at 5×10^4 cells in a 6-well plate or 5×10^5 cells in a 10-cm diameter plate with the culture medium changed to DMEM without FBS, and were precultured under serum starvation for 24–48 h. The growth-arrested ATDC5 cells were then stimulated with 5% FBS in the presence or absence of ITS (10 μg/ml insulin, 10 μg/ml transferrin, and 3×10^{-8} M sodium selenite) for 6–72 h. To block protein degradation, we added the proteasome inhibitors MG132 (2 μM, *Z*-Leu-Leu-Leu-aldehyde; Peptide Institute, Osaka, Japan) and lactacystin (20 μM, Calbiochem Novabiochem Co.) to the experimental medium, as previously reported (Urano et al., 1999; Ogasawara et al., 2004b). To block p38 MAPK, extracellular signal-regulated kinase (ERK)-1/2, and phosphatidylinositol 3 kinase (PI3K)/Akt pathways, we used SB203580 (30 μM), PD98059 (20 μM), and LY294002 (40 μM), respectively (Nakamura et al., 1999; Hidaka et al., 2001; Watanabe et al., 2001).

Construction of cell clones constitutively expressing Cdk6

ATDC5 cells were inoculated at 5×10^5 cells per 6-cm diameter plate, incubated for 24 h, and then transfected with the pEF/neo I vector carrying a human *Cdk6* cDNA or no insert by use of the Lipofectamine reagent (Life Technologies, Inc., Grand Island, NY) according to the manufacturer's instructions. Twenty-four hours later, the cells were split 1:10 to 1:100 and selected in DMEM/F12 containing 5% FBS and 200 μg/ml of G418 (Geneticin; Life Technologies, Inc.). Stable G418-resistant colonies were then isolated and expanded for 2 weeks in the medium above. The levels of Cdk6 were then quantified by Western blotting to select high expressing and low expressing clones. Cells with less than 1.5-fold of Cdk6 protein levels compared to the empty vector (EV)-transfected cells, determined by densitometry (Bio-Rad Laboratories, Richmond, CA), were defined as low expressers and those with more than fivefold of EV cells as high expressers. To know the effect of ITS on the Cdk6 overexpression level, Western blotting was performed after 5 weeks of additional culture in the presence of ITS. Cdk2 and Cdk4 levels were also examined in both situations.

Western blot analysis

The cells were rinsed with ice-cold phosphate-buffered saline (PBS) and lysed with RIPA buffer (10 mM Tris-HCl [pH 7.5], 150 mM NaCl, 1% Nonidet P-40 [NP-40], 0.1% sodium dodecyl sulfate [SDS], 10 μg of aprotinin/ml, 0.1 M NaF, 2 mM Na3VO4, and 1% Na deoxycholate). After a brief sonication, the lysed cells were centrifuged at 15,000*g* for 20 min at 4°C to obtain soluble cell extracts. The protein concentration in the cell lysate was measured using a Protein Assay Kit II (Bio-Rad). The cell extracts (10 μg of protein each) were separated by SDS-7.5, 10, or 12.5% polyacrylamide gel electrophoresis and electrotransferred to polyvinylidene difluoride membranes (Immobilon-P; Millipore Corp., Bedford, MA). After the blocking of nonspecific binding by soaking of the filters in 5% skim milk, the desired proteins were immunodetected with their respective antibodies, followed by visualization using the ECL Plus Western blotting detection system (Amersham Pharmacia Biotech, Buckinghamshire, UK) according to the manufacturer's instructions.

Reverse transcription-PCR (RT-PCR)

Total RNA (1 μg) was extracted from cells using ISOGEN (Wako Pure Chemicals, Osaka, Japan) following the manufacturer's instructions, reverse transcribed using SUPERSCRIPT First-Strand Synthesis System for RT-PCR (Life Technologies, Inc.), and amplified within an exponential phase of the amplification with a Perkin Elmer PCR Thermal Cycler (PE-2400). The gene-specific primer pairs used were as follows: 5′-CGTGGTCAGGTTGTTTGATG-3′ and 5′-TGCGAAACATTTCTGCAAAG-3′ for Cdk6, 5′-AGTAACTTCGTGCCTAGCAA-3′ and 5′-TCCTTTCACGCCTTTGAAGC-3′ for type II collagen (COL2), 5′-AGGCAAGCCAGGCTATGGAA-3′ and 5′-GCTGTCCTGGAAAGCCGTTT-3′ for type X collagen (COL10), 5′-CATGTAGGCCATGAGGTCCACCAC-3′ and 5′-TGAAGGTCGGTGTGAACGGATTTGGC-3′ for glyceraldehyde-3-phosphate dehydrogenase (GAPDH). The cycling parameters were 30 sec at 94°C, 30 sec at 55°C, and 90 sec at 72°C for Cdk6 and GAPDH; and 30 sec at 94°C, 30 sec at 60°C, and 90 sec at 72°C for COL2 and COL10.

Real-time quantitative RT-PCR

Total RNA extracted as described above was reverse-transcribed with Takara RNA PCR Kit (AMV) ver.2.1 (Takara, Tokyo, Japan) to generate single-stranded cDNA. PCR was performed with an ABI Prism 7000 Sequence Detection System (Applied Biosystems, Foster, CA). PCR reactions consisted of 1× QuantiTect SYBR Green PCR Master Mix (Qiagen, Hilden, Germany), 0.3 μM specific primers, and 500 ng of cDNA. mRNA copy number of a specific gene in each total RNA was calculated with a standard curve generated with serially diluted plasmids containing PCR amplicon sequences, and normalized to the rodent total RNA (Applied Biosystems) with β-actin as an internal control. Standard plasmids were synthesized with TOPO TA Cloning Kit (Invitrogen, Carlsbad, CA) according to the manufacturer's instruction. All reactions were run in triplicate. Primer sequences for Sox5 were, sense (5′-CTCGCTGGAAAGCTATGACC-3′) and antisense (5′-GATGGGGATCTGTGCTTGTT-3′), for Sox6 were, sense (5′-GGATTGGG- GAGTACAAGCAA-3′) and antisense (5′-CATCTGAGGTGATGGTGTGG-3′), for Sox9 were, sense (5′-CGACTACGCTGACCATCAGA-3′) and antisense (5′-AGACTGGTTGTTCCCAGTGC-3′), and for β-actin were, sense(5′-AGATGTGGATCAGCAAGCAG-3′) and antisense (5′-GCGCAAGTTAGGTTTTGTCA-3′).

Alcian blue, alizarin red, and alkaline phosphatase (ALP) stainings

ATDC5 cells were inoculated at 5×10^4 cells per well in a 6-well plate and cultured in DMEM/F12 containing 5% FBS in 5% CO_2 in air. After being cultured to be subconfluent, the cells were induced for differentition by adding 10 μg/ml ITS and cultured for 3 weeks, then the culture medium was changed to α-minimum essential medium (αMEM; Life Technologies, Inc.) containing 5% FBS with ITS, and the cells were cultured in 3% CO_2 in air for more 2 weeks. Alcian blue staining was done at 3 weeks after induction of chondrogenesis, and Alizarin red and ALP stainings at 5 weeks. For Alcian blue staining, the cells were rinsed with PBS, fixed with 10% (vol/vol) formaldehyde, and stained with 0.3% Alcian blue 8GS (Fluka, Buchs, Switzerland) in 0.1 N HCl. For Alizarin red staining, the cells were rinsed with PBS and fixed with 10% (vol/vol) formaldehyde, and were stained

with 1% Alizarin red S (pH 4.0) (Sigma). For ALP staining, the cells were rinsed with PBS and fixed with 70% ethanol in PBS and then stained with naphthol AS-MX phosphate (Sigma) as a substrate in *N,N*-dimethyl formamide, and Fast BB salt (Sigma) as a coupler.

BrdU incorporation assay

ATDC5 cells were inoculated at 10^3 cells per well in a 96-well plate and cultured in DMEM/F12 containing 5% FBS with or without ITS. After 72 h of culture, the cells were labeled with bromodeoxyuridine (BrdU) for 2 h, and the cell population entering S-phase was determined by quantifying the incorporated BrdU (Cell Proliferation ELISA; Roche Molecular Biochemical) according to the manufacturer's instructions.

Flow cytometric analysis

After 72 h of culture, approximately 10^5 cells were suspended in 0.02 ml of citrate buffer and subjected to the following serial treatments at room temperature: (i) the addition of 0.18 ml of solution A (0.03 mg of trypsin/ml, 3.4 mM trisodium citrate, 0.1% NP-40, 1.5 mM spermine-4HCl, and 0.5 mM Tris-HCl [pH 7.6]) and incubation for 10 min; (ii) the addition of 0.15 ml of solution B (3.4 mM trisodium citrate, 0.1% NP-40, 1.5 mM spermine-4HCl, 0.5 mM Tris-HCl [pH 7.6], 0.5 mg of trypsin inhibitor/ml, 0.1 mg of RNase A/ml) and incubation for 10 min; and (iii) the addition of 0.15 ml of solution C (4.16 mg of propidium iodide/ml, 3.4 mM trisodium citrate, 0.1% NP-40, 4.8 mM spermine-4HCl, 0.5 mM Tris-HCl [pH 7.6]) and incubation for 10 min. The DNA content was determined and analyzed with EPICS XL and XL EXPO32 instruments (Beckman, Fullerton, CA).

Statistical analysis

The means of groups were compared by analysis of variance, and the significance of differences was determined by posthoc testing using the Bonferroni method.

RESULTS

Downregulation of Cdk6 during differentiation of ATDC5 cells

Considering that ATDC5 cells begin to express COL2, a representative marker of chondrocytes, within 72–96 h of culture in the medium containing ITS, a putative inducer of chondrocyte differentiation (Shukunami et al., 1996, 1998), we assumed that the commitment of this cell line to differentiation occurred well within 72 h, and therefore analyzed the effect of ITS on the initial 72 h expression levels of cell cycle factors that critically regulate the onset of S-phase. The cells were arrested in quiescence by serum starvation, stimulated with serum in the presence or absence of ITS, and the amounts of cyclins (A, D1, D2, D3, and E), Cdk2, Cdk4, Cdk6, and CKIs (p15, p16, p18, p19, p21, p27, and p57) in the whole cell lysate at each time point were analyzed every 12–24 h by Western blotting (Fig. 1A). Interestingly, only Cdk6 protein level was significantly decreased by ITS at 24 h of culture and thereafter, while other Cdks, cyclins, and CKIs were hardly affected by the stimulation. Although Cdk4 and Cdk6 have about 70% homology of amino acid sequence (Meyerson et al., 1992) and share D cyclins as their catalytic partners, only Cdk6 was regulated, indicating that Cdk6 was specifically downregulated during the chondrocyte differentiation. To know the regulation of Cdk6 at the transcriptional level, we performed a semiquantitative RT-PCR analysis of the Cdk6 transcript and found that the mRNA level was also decreased when ATDC5 cells were stimulated with ITS (Fig. 1B). To further examine the involvement of the ubiquitin-proteasome pathway in the decreased Cdk6 protein level, ATDC5 cells were cultured with MG132 and lactacystin, potent proteasome inhibitors (Fig. 1C). These inhibitors did not affect the Cdk6 downregulation by ITS, suggesting that the effect of ITS was not due

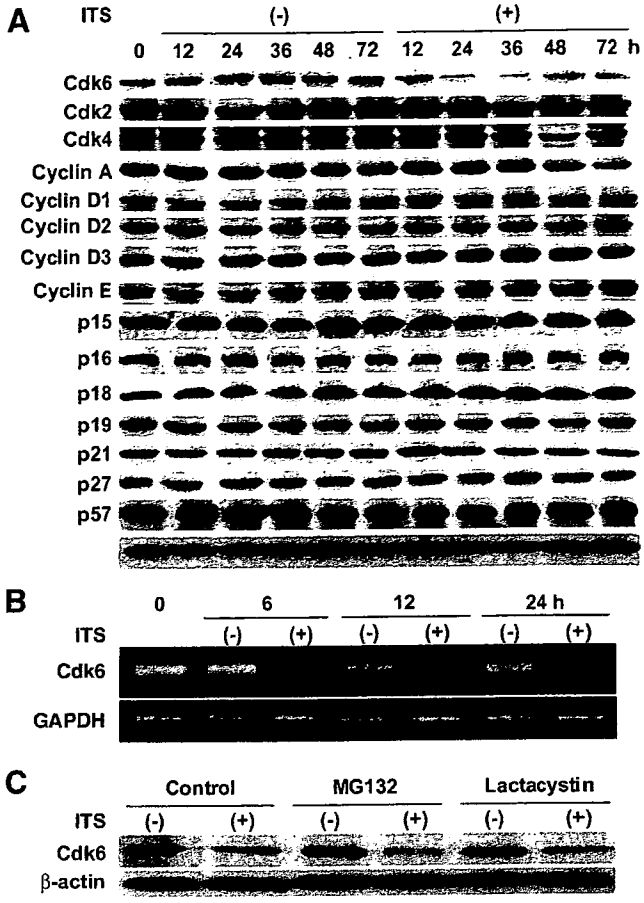

Fig. 1. Downregulation of Cdk6 during differentiation of ATDC5 cells. Growth-arrested ATDC5 cells were stimulated with 5% FBS in the presence or absence of ITS, a putative inducer of chondrocyte differentiation, and cell sampling was done at the indicated times. **A**: Time course of protein levels of cell cycle factors Cdks, cyclins, and CKIs, controlling the G1-S transition in ATDC5 cells during differentiation induction by ITS. The amounts of cell cycle factors were determined by Western blotting. β-actin was used as a loading control. **B**: Time course of the mRNA level of Cdk6 by a semiquantitative RT-PCR analysis in ATDC5 cells during differentiation by ITS. GAPDH was used as a loading control. **C**: Effects of proteasome inhibitors MG132 (2 μM) and lactacystin (20 μM) on the decreased Cdk6 protein level determined by Western blotting during ATDC5 cell differentiation by ITS. Growth-arrested ATDC5 cells were stimulated for 24 h, and the amounts were determined by Western blotting. β-actin was used as a loading control. In each figure a representative blotting is shown among at least three independent experiments that showed similar results.

to protein degradation by the ubiquitin-proteasome pathway. These findings indicate that the decreased Cdk6 expression during chondrocyte differentiation was mainly, if not exclusively, by transcriptional suppression.

Mediation of p38 MAPK in the downregulation of Cdk6

Since insulin, the principal factor in ITS for chondrocyte differentaition, is known to initiate cellular responses by binding to distinct cell-surface receptor tyrosine kinases that regulate a variety of signaling pathways such as those of MAPK and PI3K/Akt (Kadowaki et al., 1996), we examined the involvement of these pathways in the mechanism of the Cdk6 downregulation by ITS. Western blotting showed that ITS induced the phosphyrylation of p38 MAPK in cultured ATDC5 cells, which was confirmed to be

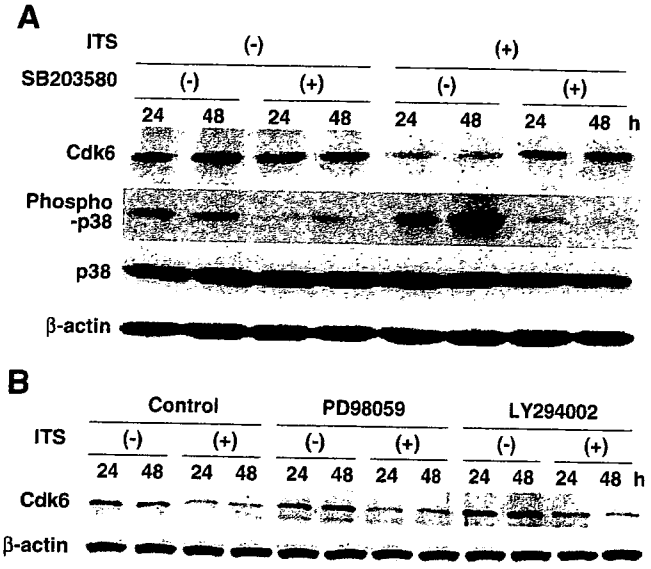

Fig. 2. Mediation of p38 MAPK, ERK-1/2, and PI3K/Akt pathways in the downregulation of Cdk6 during differentiation of ATDC5 cells. **A**: Effects of ITS and a p38 MAPK inhibitor SB203580 on the Cdk6 protein level and the p38 MAPK phosphorylation in the ATDC5 cell cultures. Growth-arrested ATDC5 cells were stimulated for 24 and 48 h, and the amounts were determined by Western blotting using specific antibodies. **B**: Effects of PD98059 and LY294002, inhibitors of ERK-1/2 and PI3K/Akt signalings, respectively, on the decreased Cdk6 protein level during ATDC5 cell differentiation by ITS. Growth-arrested ATDC5 cells were stimulated for 24 and 48 h, and the amounts were determined by Western blotting. In each figure a representative blotting is shown among at least four independent experiments that showed similar results. β-actin was used as a loading control.

blocked by SB203580, a p38 MAPK inhibitor (Fig. 2A). More importantly, SB203580 caused the restoration of the decreased Cdk6 protein level by ITS (Fig. 2A). On the other hand, PD98059 and LY294002, inhibitors of ERK-1/2 and PI3K/Akt signalings, respectively, did not alter the ITS-induced inhibition of the Cdk6 protein level (Fig. 2B). These findings demonstrate that downregulation of Cdk6 expression by ITS is at least partly mediated by the p38 MAPK pathway.

Impaired differentiation of ATDC5 cells overexpressing Cdk6

To further examine whether or not Cdk6 is functionally involved in chondrocyte differentiation, we generated ATDC5 cell clones stably overexpressing Cdk6 by transfecting with an expressing vector harboring *Cdk6* cDNA, and tested their ability to respond to ITS and differentiate to chondrocytes. We initially selected clones with low expression (#55 and #74) and high expression (#14 and #51), and confirmed that these overexpressions were maintained even after 5 weeks of culture in the presence of ITS (Fig. 3A). These overexpressions of Cdk6 affected neither the Cdk2 nor Cdk4 expression profiles even after long periods of culture with ITS (Fig. 3A). The ability of ITS to induce differentiation determined by Alcian blue, Alizarin red, and ALP stainings was then compared among the EV-transfected cells, low expressing cells, and high expressing cells after 3–5 weeks of culture. ITS induced the differentiation similarly in EV cells and low expressers; however, it was markedly decreased in high expressers (Fig. 3B). The ability of ITS to induce chondrocyte differentiation, as monitored by COL2 (Fig. 3C) and COL10 (Fig. 3D) mRNA levels by semiquantitative RT-PCR was further studied in the three kinds of transfected cells above. Here again, ITS strongly induced both COL2 and COL10 in the EV cells and low expressers, which was markedly decreased in high expressers. We further compared the expressions of Sox 5, Sox6, and Sox9, the key transcription factors for chondrogenic differentiation from precursors (Bi et al., 1999; Smits et al., 2001) by real-time quantitative RT-PCR analysis among the three kinds of transfected cells that were cultured for 24 h in the presence of ITS. The mRNA levels of Sox5 and Sox6, but not Sox9, were significantly lower in the high expressers than other two kinds of cells, indicating that Cdk6 exerts inhibitory action from an early stage of chondrocyte differentiation (Fig. 3E).

Unchanged cell cycle regulation of ATDC5 cells overexpressing Cdk6

Because Cdk6 promotes the G1-S transition, suppression of chondrocyte differentiation by overexpressed Cdk6 could be secondary to its execution of this role. We therefore examined the effect of Cdk6 overexpression on the proliferation and the G1-S transition of ATDC5 cells. The three kinds of transfected cells were similarly arrested in quiescence, stimulated with serum in the presence and absence of ITS, and analyzed for cell proliferation and populations in G0/G1 and G2/M by BrdU incorporation and FACS, respectively (Table 1). At 72 h of culture, when chondrocyte differentiation had just begun, ITS slightly increased the cell proliferation and the G2/M population; however, Cdk6 overexpression caused no significant changes in either of them. These results indicate that the inhibitory effect of Cdk6 on chondrocyte differentiation was not exerted via the cell cycle regulation.

DISCUSSION

In the present study, we have shown that Cdk6 expression is suppressed during differentiation of mouse prechondrocyte ATDC5 mainly at the transcriptional level and that this suppression, mediated by p38 MAPK signaling, is involved in the efficient differentiation. The work has demonstrated that Cdk6 plays a role in determining the differentiation rate of chondrocytes as a downstream effector of p38 MAPK signaling.

Although Cdk6 and Cdk4 and their partner D cyclins are all known to be critical factors controlling the cell growth potential (Baldin et al., 1993; Hengstschlager et al., 1999), several specific roles have been reported for Cdk6. The Cdk6–cyclin D3 complex is unique among cyclin D and cognate kinase combinations and evades inhibition by CKIs (Lin et al., 2001). Therefore, it can greatly enhance the proliferative potential of fibroblasts under growth-suppressive conditions (Lin et al., 2001) and, consequently, sensitizes cells to physical and chemical transformation (Chen et al., 2003). Cdk6 combined with cyclin K, encoded by human herpes virus 8 which is the causative agent of Kaposi sarcoma, is also reported to be immune to inhibition by CKIs (Swanton et al., 1997). These functions were not seen in Cdk4 complexes. This study also discovered a novel function of Cdk6 as an inhibitor of the transition to the differentiation stage without affecting the cell cycle regulation. Although Cdk4 has about 70% homology of amino acid sequence with Cdk6 (Meyerson et al., 1992), the Cdk4 protein level was not changed during ATDC5 differentiation in this study. We hereby propose that Cdk4 and Cdk6 play different roles and that Cdk4 cannot substitute for Cdk6 in chondrocyte differentiation.

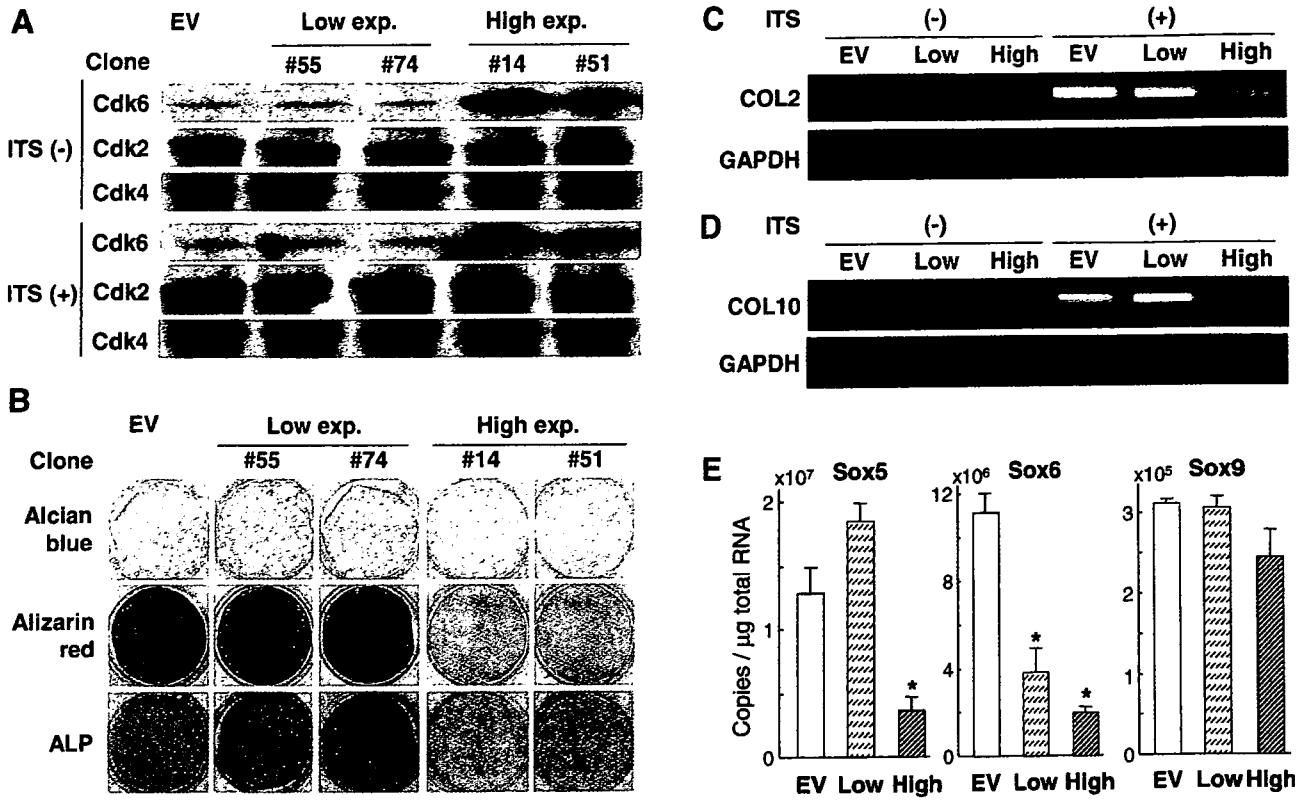

Fig. 3. Chondrocyte differentiation of ATDC5 cells with high and low expressions of Cdk6. **A**: Stable clones of ATDC5 cells transfected with *Cdk6* cDNA were isolated as described in Materials and Methods, and clones with low expression (#55 and #74) and high expression (#14 and #51) were selected on Western blotting after 2 weeks of expansion culture in the absence of ITS [ITS (−)]. To examine the effect of ITS on the Cdk6 overexpression, Western blotting was performed after 5 weeks of additional culture in the presence of ITS [ITS (+)]. **B**: Chondrocyte differentiation determined by Alcian blue, Alizarin red, and ALP stainings in the cultures of the low and high expressing clones, and empty vector (EV)-transfected ATDC5 cells under the induction of ITS for 3–5 weeks. **C, D**: mRNA levels of COL2 (C) and COL10 (D), as determined by semiquantitative RT-PCR, in EV cells, low expressers (#55), and high expressers (#14) cultured for 3 days and 14 days, respectively, in the presence or absence of ITS. GAPDH was used as a loading control. **E**: Expressions of Sox 5, Sox6, and Sox9, as determined by real-time quantitative RT-PCR analysis in EV cells, low expressers (#55), and high expressers (#14) cultured for 24 h in the presence of ITS. For (B–E), other clones with low and high expressions showed similar results.

The direct control of a factor(s) critically involved in the differentiation that is independent of cell cycle regulation, implicated as a Cdk6 action in this study, may not be as remote as generally thought. In fission yeast, Pas1 cyclin and its partner kinase Pef1 activate a transcriptional factor complex functionally equivalent to E2F-DP of mammals, thereby promoting S-phase entry just like Cdk6, yet they independently inhibit the mating pheromone signaling whose activation is essential for differentiation of this yeast cell (Tanaka and Okayama, 2000). Thus, this might be a good preceding model for the situation of Cdk6 in chondrocyte differentiation, highlighting a potential functional similarity between Cdk6 and Pef1.

Since Cdks are believed to have vital roles in controlling cell cycle progression among cell cycle factors, much attention has been devoted to the view that CKI-led inhibition of G1-specific Cdks is critical for cell differentiation. Recent reports have stated that some members of CKIs may function during the exit from the cell cycle and differentiation processes (Harper and Elledge, 1996; Chellappan et al., 1998). Overexpression of p21 and p27 has, in fact, promoted myogenesis, neurogenesis, and hematopoiesis (Liu

TABLE 1. Proliferation and cell cycle distribution of ATDC5 cells overexpressing Cdk6

	BrdU (OD)		FACS			
			G0/G1 (%)		G2/M (%)	
	ITS (−)	ITS (+)	ITS (−)	ITS (+)	ITS (−)	ITS (+)
EV	0.25 ± 0.01	0.35 ± 0.10	66.0 ± 0.6	62.7 ± 0.8	20.9 ± 0.2	23.6 ± 0.7
#55 (low)	0.23 ± 0.05	0.35 ± 0.09	65.6 ± 1.1	63.9 ± 0.7	22.4 ± 0.9	23.7 ± 0.5
#74 (low)	0.23 ± 0.03	0.39 ± 0.10	66.1 ± 0.1	64.8 ± 0.6	20.6 ± 0.5	22.5 ± 0.7
#14 (high)	0.20 ± 0.04	0.34 ± 0.11	66.3 ± 1.1	65.2 ± 0.5	20.4 ± 0.2	21.8 ± 0.7
#51 (high)	0.25 ± 0.01	0.36 ± 0.04	64.7 ± 1.2	62.6 ± 1.0	22.7 ± 0.3	24.7 ± 0.3

Cell proliferation was determined by BrdU incorporation into EV, low expressing and high expressing clones in the presence and absence of ITS at 72 h of culture. Cell cycle distribution was determined by FACS at 72 h of culture, and percentage of cells in each cell cycle stage (G0/G1 and G2/M) are shown. Data are expressed as the mean ± SD for 8 wells/clone. Cdk6 overexpression did not significantly affect the cell proliferation and the cell cycle distribution.

et al., 1996; Matsumura et al., 1997; Erhardt and Pittman, 1998; Ohnuma et al., 1999). Several studies revealed a certain correlation between induction of p21 and differentiation in hematopoietic cells including monocytes/macrophages (Steinman et al., 1994; Schwaller et al., 1995; Liu et al., 1996). For chondrocytes as well, p57 and p21 have been reported to play certain roles (Beier et al., 1999b; Aikawa et al., 2001; MacLean et al., 2004; Stewart et al., 2004). Mice lacking *p57* have major developmental defects, including body wall dysplasia and short limbs with elevated chondrocyte proliferation rate, increased chondrocyte cell density, and delayed ossification (Yan et al., 1997; Zhang et al., 1997). It is, however, known that the inhibitory effect of p57 over cyclin D/Cdk6 is much weaker than that over other cyclin/Cdk complexes (Matsuoka et al., 1995), so that the function of Cdk6 as a differentiation inhibitor may not be mediated by p57. Other cell cycle factors known to be required by chondrocytes during early development are the Rb-related pocket proteins, p107 and p130, since mice lacking both *p107* and *p130* have a bone phenotype very similar to that of the *p57*-mutant embryos (Cobrinik et al., 1996; Rossi et al., 2002). Because Cdk6 can at least bind to both p107 and p130, although the functional associations remain unclear (Grana et al., 1998), Cdk6 might possibly influence chondrocyte differentiation by interacting with these pocket proteins.

Using the same ATDC5 cell culture system as the present study, a group under Negishi and Nakajima has shown that an increase in p21 expression through ERK1/2 and p38 MAPK is required for the differentiation (Negishi et al., 2001; Nakajima et al., 2004), which sounds inconsistent with the present results that p21 protein level was not altered during the ATDC5 differentaition (Fig. 1A). The discrepancy may lie in the difference of the culture period: the p21 was increased only after 5 days and was not seen within 3 days in their study, while Cdk6 was inhibited as early as 24 h in our study. It is of note that the suppression of Cdk6 protein level seems transient, but not consistent, since it somewhat recovered at 48 h and thereafter (Fig. 1A). We therefore speculate that chondrocyte differentiation might be regulated by sequential actions of several cell cycle factors, in which Cdk6 plays a role at earlier stages for the induction of the G1 arrest while p21 at later stages. However, the fact that mice lacking p21 develop and grow normally without significant skeketal abnormality strongly refutes its importance for chondrocyte differentiation in vivo (Deng et al., 1995). Regarding Cdk6 in vivo, a recent report showed that Cdk6-null female mice were smaller than their wild-type littermates (Malumbres et al., 2004). Furthermore, our preliminary study showed that transgenic mice that overexpress Cdk6 and cyclin D1 under the control of COL2 promoter/enhancer display dwarfism with impaired chondrocyte maturation in the growth plate.

This study for the first time demonstrated that Cdk6, a G1 cell cycle factor, may play a role in controlling chondrocyte differentiation. Interstingly, Cdk6 overexpression was not associated with the Sox9 level, but decreased the Sox5 and Sox6 levels (Fig. 3E). Considering that Sox9 is essential for the condensation of mesenchyme cells that is prerequisite for the chondrogenic differentiation while Sox5 and Sox6 are needed thereafter as the co-activators (Bi et al., 1999; Smits et al., 2001), Cdk6 may contribute to the early stage of chondrogenic differentiation like commitment of precursors to the lineage. Decrease in several stainings, COL2 and COL10 (Fig. 3B–D), might possibly be secondary to the inhibition at the early stage. Identification of the transcriptional repressor as well as key targets for Cdk6 will be helpful for deeper understanding of the molecular basis of chondrocyte differentiation.

Finally, it should be noted that our finding is not specific to the differentiation of chondrocytes. Matushansky et al. (2003) reported that downregulation of Cdk6 is required for the erythroid differentiation of a murine leukemia cell line. Recently, we also demonstrated a similar role of Cdk6 in the osteoblast and osteoclast differentiations through Smad and NF-κB signalings, respectively (Ogasawara et al., 2004a,b). We therefore propose that Cdk6 might be a common molecule that regulates the transition to the differentiation stage in several cells, as an effector of the distinct signalings.

ACKNOWLEDGMENTS

We thank Reiko Yamaguchi for providing expert technical assistance.

LITERATURE CITED

Aikawa T, Segre GV, Lee K. 2001. Fibroblast growth factor inhibits chondrocytic growth through induction of p21 and subsequent inactivation of cyclin E-Cdk2. J Biol Chem 276:29347–29352.

Baldin V, Lukas J, Marcote MJ, Pagano M, Draetta G. 1993. Cyclin D1 is a nuclear protein required for cell cycle progression in G1. Genes Dev 7:812–821.

Beier F, Leask TA, Haque S, Chow C, Taylor AC, Lee RJ, Pestell RG, Ballock RT, LuValle P. 1999a. Cell cycle genes in chondrocyte proliferation and differentiation. Matrix Biol 18:109–120.

Beier F, Taylor AC, LuValle P. 1999b. The Raf-1/MEK/ERK pathway regulates the expression of the p21(Cip1/Waf1) gene in chondrocytes. J Biol Chem 274:30273–30279.

Bi W, Deng JM, Zhang Z, Behringer RR, de Crombrugghe B. 1999. Sox9 is required for cartilage formation. Nat Genet 22:85–89.

Chellappan SP, Giordano A, Fisher PB. 1998. Role of cyclin-dependent kinases and their inhibitors in cellular differentiation and development. Curr Top Microbiol Immunol 227:57–103.

Chen Q, Lin J, Jinno S, Okayama H. 2003. Overexpression of Cdk6-cyclin D3 highly sensitizes cells to physical and chemical transformation. Oncogene 22:992–1001.

Cobrinik D, Lee MH, Hannon G, Mulligan G, Bronson RT, Dyson N, Harlow E, Beach D, Weinberg RA, Jacks T. 1996. Shared role of the pRB-related p130 and p107 proteins in limb development. Genes Dev 10:1633–1644.

Coqueret O. 2002. Linking cyclins to transcriptional control. Gene 299:35–55.

Deng C, Zhang P, Harper JW, Elledge SJ, Leder P. 1995. Mice lacking p21CIP1/WAF1 undergo normal development, but are defective in G1 checkpoint control. Cell 82:675–684.

Erhardt JA, Pittman RN. 1998. Ectopic p21(WAF1) expression induces differentiation-specific cell cycle changes in PC12 cells characteristic of nerve growth factor treatment. J Biol Chem 273:23517–23523.

Grana X, Garriga J, Mayol X. 1998. Role of the retinoblastoma protein family, pRB, p107 and p130 in the negative control of cell growth. Oncogene 17:3365–3383.

Harper JW, Elledge SJ. 1996. Cdk inhibitors in development and cancer. Curr Opin Genet Dev 6:56–64.

Hengstschlager M, Braun K, Soucek T, Miloloza A, Hengstschlager-Ottnad E. 1999. Cyclin-dependent kinases at the G1-S transition of the mammalian cell cycle. Mutat Res 436:1–9.

Hidaka K, Kanematsu T, Takeuchi H, Nakata M, Kikkawa U, Hirata M. 2001. Involvement of the phosphoinositide 3-kinase/protein kinase B signaling pathway in insulin/IGF-I-induced chondrogenesis of the mouse embryonal carcinoma-derived cell line ATDC5. Int J Biochem Cell Biol 33:1094–1103.

Kadowaki T, Tobe K, Honda-Yamamoto R, Tamemoto H, Kaburagi Y, Momomura K, Ueki K, Takahashi Y, Yamauchi T, Akanuma Y, Yazaki Y. 1996. Signal transduction mechanism of insulin and insulin-like growth factor-1. Endocr J 43 (Suppl):S33–S41.

Karsenty G, Wagner EF. 2002. Reaching a genetic and molecular understanding of skeletal development. Dev Cell 2:389–406.

Lin J, Jinno S, Okayama H. 2001. Cdk6-cyclin D3 complex evades inhibition by inhibitor proteins and uniquely controls cell's proliferation competence. Oncogene 20:2000–2009.

Liu M, Lee MH, Cohen M, Bommakanti M, Freedman LP. 1996. Transcriptional activation of the Cdk inhibitor p21 by vitamin D3 leads to the induced differentiation of the myelomonocytic cell line U937. Genes Dev 10:142–153.

LuValle P, Beier F. 2000. Cell cycle control in growth plate chondrocytes. Front Biosci 5:D493–D503.

MacLean HE, Guo J, Knight MC, Zhang P, Cobrinik D, Kronenberg HM. 2004. The cyclin-dependent kinase inhibitor p57(Kip2) mediates proliferative actions of PTHrP in chondrocytes. J Clin Invest 113:1334–1343.

Malumbres M, Sotillo R, Santamaria D, Galan J, Cerezo A, Ortega S, Dubus P, Barbacid M. 2004. Mammalian cells cycle without the D-type cyclin-dependent kinases Cdk4 and Cdk6. Cell 118:493–504.

Matsumura I, Ishikawa J, Nakajima K, Oritani K, Tomiyama Y, Miyagawa J, Kato T, Miyazaki H, Matsuzawa Y, Kanakura Y. 1997. Thrombopoietin-induced differentiation of a human megakaryoblastic leukemia cell line, CMK,

involves transcriptional activation of p21(WAF1/Cip1) by STAT5. Mol Cell Biol 17:2933–2943.
Matsuoka S, Edwards MC, Bai C, Parker S, Zhang P, Baldini A, Harper JW, Elledge SJ. 1995. p57KIP2, a structurally distinct member of the p21CIP1 Cdk inhibitor family, is a candidate tumor suppressor gene. Genes Dev 9:650–662.
Matushansky I, Radparvar F, Skoultchi AI. 2003. CDK6 blocks differentiation: Coupling cell proliferation to the block to differentiation in leukemic cells. Oncogene 22:4143–4149.
Meyerson M, Enders GH, Wu CL, Su LK, Gorka C, Nelson C, Harlow E, Tsai LH. 1992. A family of human cdc2-related protein kinases. EMBO J 11:2909–2917.
Mundlos S, Olsen BR. 1997a. Heritable diseases of the skeleton. Part I: Molecular insights into skeletal development-transcription factors and signaling pathways. FASEB J 11:125–132.
Mundlos S, Olsen BR. 1997b. Heritable diseases of the skeleton. Part II: Molecular insights into skeletal development-matrix components and their homeostasis. FASEB J 11:227–233.
Nakajima M, Negishi Y, Tanaka H, Kawashima K. 2004. p21(Cip-1/SDI-1/WAF-1) expression via the mitogen-activated protein kinase signaling pathway in insulin-induced chondrogenic differentiation of ATDC5 cells. Biochem Biophys Res Commun 320:1069–1075.
Nakamura K, Shirai T, Morishita S, Uchida S, Saeki-Miura K, Makishima F. 1999. p38 mitogen-activated protein kinase functionally contributes to chondrogenesis induced by growth/differentiation factor-5 in ATDC5 cells. Exp Cell Res 250:351–363.
Negishi Y, Ui N, Nakajima M, Kawashima K, Maruyama K, Takizawa T, Endo H. 2001. p21Cip-1/SDI-1/WAF-1 gene is involved in chondrogenic differentiation of ATDC5 cells in vitro. J Biol Chem 276:33249–33256.
Ogasawara T, Katagiri M, Yamamoto A, Hoshi K, Takato T, Nakamura K, Tanaka S, Okayama H, Kawaguchi H. 2004a. Osteoclast differentiation by RANKL requires NF-kappaB-mediated downregulation of cyclin-dependent kinase 6 (Cdk6). J Bone Miner Res 19:1128–1136.
Ogasawara T, Kawaguchi H, Jinno S, Hoshi K, Itaka K, Takato T, Nakamura K, Okayama H. 2004b. Bone morphogenetic protein 2-induced osteoblast differentiation requires Smad-mediated down-regulation of Cdk6. Mol Cell Biol 24:6560–6568.
Ohnuma S, Philpott A, Wang K, Holt CE, Harris WA. 1999. p27Xic1, a Cdk inhibitor, promotes the determination of glial cells in Xenopus retina. Cell 99:499–510.
Rossi F, MacLean HE, Yuan W, Francis RO, Semenova E, Lin CS, Kronenberg HM, Cobrinik D. 2002. p107 and p130 Coordinately regulate proliferation, Cbfa1 expression, and hypertrophic differentiation during endochondral bone development. Dev Biol 247:271–285.
Schwaller J, Koeffler HP, Niklaus G, Loetscher P, Nagel S, Fey MF, Tobler A. 1995. Posttranscriptional stabilization underlies p53-independent induction of p21WAF1/CIP1/SDI1 in differentiating human leukemic cells. J Clin Invest 95:973–979.
Serra R, Johnson M, Filvaroff EH, LaBorde J, Sheehan DM, Derynck R, Moses HL. 1997. Expression of a truncated, kinase-defective TGF-beta type II receptor in mouse skeletal tissue promotes terminal chondrocyte differentiation and osteoarthritis. J Cell Biol 139:541–552.
Sherr CJ. 1994. G1 phase progression: Cycling on cue. Cell 79:551–555.
Sherr CJ, Roberts JM. 1999. CDK inhibitors: Positive and negative regulators of G1-phase progression. Genes Dev 13:1501–1512.
Shukunami C, Shigeno C, Atsumi T, Ishizeki K, Suzuki F, Hiraki Y. 1996. Chondrogenic differentiation of clonal mouse embryonic cell line ATDC5 in vitro: Differentiation-dependent gene expression of parathyroid hormone (PTH)/PTH-related peptide receptor. J Cell Biol 133:457–468.
Shukunami C, Ohta Y, Sakuda M, Hiraki Y. 1998. Sequential progression of the differentiation program by bone morphogenetic protein-2 in chondrogenic cell line ATDC5. Exp Cell Res 241:1–11.
Smits P, Li P, Mandel J, Zhang Z, Deng JM, Behringer RR, de Crombrugghe B, Lefebvre V. 2001. The transcription factors L-Sox5 and Sox6 are essential for cartilage formation. Dev Cell 1:277–290.
Steinman RA, Hoffman B, Iro A, Guillouf C, Liebermann DA, el-Houseini ME. 1994. Induction of p21 (WAF-1/CIP1) during differentiation. Oncogene 9:3389–3396.
Stewart MC, Kadlcek RM, Robbins PD, MacLeod JN, Ballock RT. 2004. Expression and activity of the CDK inhibitor p57Kip2 in chondrocytes undergoing hypertrophic differentiation. J Bone Miner Res 19:123–132.
Swanton C, Mann DJ, Fleckenstein B, Neipel F, Peters G, Jones N. 1997. Herpes viral cyclin/Cdk6 complexes evade inhibition by CDK inhibitor proteins. Nature 390:184–187.
Tanaka K, Okayama H. 2000. A pcl-like cyclin activates the Res2p-Cdc10p cell cycle "start" transcriptional factor complex in fission yeast. Mol Biol Cell 11:2845–2862.
Urano T, Yashiroda H, Muraoka M, Tanaka K, Hosoi T, Inoue S, Ouchi Y, Toyoshima H. 1999. p57(Kip2) is degraded through the proteasome in osteoblasts stimulated to proliferation by transforming growth factor beta1. J Biol Chem 274:12197–12200.
Watanabe H, de Caestecker MP, Yamada Y. 2001. Transcriptional cross-talk between Smad, ERK1/2, and p38 mitogen-activated protein kinase pathways regulates transforming growth factor-beta-induced aggrecan gene expression in chondrogenic ATDC5 cells. J Biol Chem 276: 14466–14473.
Yan Y, Frisen J, Lee MH, Massague J, Barbacid M. 1997. Ablation of the CDK inhibitor p57Kip2 results in increased apoptosis and delayed differentiation during mouse development. Genes Dev 11:973–983.
Zhang P, Liegeois NJ, Wong C, Finegold M, Hou H, Thompson JC, Silverman A, Harper JW, DePinho RA, Elledge SJ. 1997. Altered cell differentiation and proliferation in mice lacking p57KIP2 indicates a role in Beckwith–Wiedemann syndrome. Nature 387:151–158.

OsteoArthritis and Cartilage (2005) **13**, 632–641

doi:10.1016/j.joca.2005.03.004

Osteoarthritis and Cartilage

ICRS International Cartilage Repair Society

OARSI OSTEOARTHRITIS RESEARCH SOCIETY INTERNATIONAL

Osteoarthritis development in novel experimental mouse models induced by knee joint instability

S. Kamekura M.D.†, K. Hoshi M.D., Ph.D.‡, T. Shimoaka M.D., Ph.D.†, U. Chung M.D., Ph.D.‡, H. Chikuda M.D., Ph.D.‡, T. Yamada M.D., Ph.D.†, M. Uchida Ph.D.§, N. Ogata M.D.†, A. Seichi M.D., Ph.D.†, K. Nakamura M.D., Ph.D.† and H. Kawaguchi M.D., Ph.D.†*

† *Department of Orthopaedic Surgery, University of Tokyo, Tokyo, Japan*

‡ *Department of Tissue Engineering, Faculty of Medicine, University of Tokyo, Tokyo, Japan*

§ *Biomedical Research Laboratory, Kureha Chemical Industry Co., Ltd., Tokyo, Japan*

Summary

Objective: Although osteoarthritis (OA) is induced by accumulated mechanical stress to joints, little is known about the underlying molecular mechanism. To apply approaches from mouse genomics, this study created experimental mouse OA models by producing instability in the knee joints.

Methods: The models were of four types: severe, moderate, mild, and medial, depending on the severity and direction of instability imposed by combinations of ligament transection and menisectomy. OA development was evaluated by X-ray and histology by Safranin-O staining, and quantified using our original gradings. Expressions of type II, IX and X collagens and matrix metalloproteinase (MMP)-2, -3, -9 and -13 were further examined by immunohistochemistry and in situ hybridization (ISH).

Results: The severe, moderate and mild models exhibited OA development in the posterior tibial cartilage. The severe model showed cartilage destruction at 2 weeks and osteophyte formation at 4–8 weeks after surgery; however, the mild model showed only a partial cartilage destruction at 8 weeks. The grading confirmed that the OA disorders progressed depending on the severity of joint instability. In the medial model, the OA development in the medial tibial cartilage was similar to that in the posterior cartilage of the mild model. Among the collagens and MMPs, type X collagen and MMP-13 were markedly induced and colocalized in the early stage OA cartilage.

Conclusion: We established four types of mouse models exhibiting various speeds of OA progression. By applying a mouse genomics approach to the models, molecular backgrounds in various stages of OA development can be clarified.

Key words: Osteoarthritis, Mechanical stress, Mouse, Chondrocyte, Hypertrophy, MMP-13.

Introduction

Osteoarthritis (OA), a chronic degenerative joint disorder characterized by articular cartilage destruction and osteophyte formation, is prevalent in society as a major cause of disability. In Western countries, 10–50% of the senior population is affected by OA, a quarter of whom are severely disabled due to joint symptoms[1,2]. In Japan as well, approximately 10 million of the country's 120 million inhabitants are suffering from OA, with the figure increasing by nine hundred thousands every year. Because of the prevalence of the disease in the elderly, this trend is occurring worldwide as a consequence of increasing longevity due to the overall improvement in living conditions and health status[3]. Despite significant social demand, research on OA is still marginalized within biomedical research, so that the cellular and molecular bases for the disease are largely unmapped. Risk factors of OA so far identified by previous epidemiologic studies are limited to age, trauma history, occupation and gender[4]. Since these factors are closely related to the mechanical loading to the joints, it is assumed that a large part of OA is induced by accumulated mechanical stress. In efforts to clarify the mechanisms by which the stress lead to OA development, animal models of OA induced by producing instability of joints through surgical intervention have been developed in dogs, rabbits, guinea pigs and rats[5–8].

Due to rapid progress of mouse genomics and the availability of transgenic and knockout mice, the mouse is now the most ideal animal model for the study of molecular backgrounds of physiological and pathological conditions. There are actually several mouse OA models: spontaneous models exhibiting OA with aging such as STR/ort mouse[9] and C57 black mice[10], and gene-manipulated mice such as Del1[11]. However, since most of these models exhibit other cartilage disorders such as chondrodysplasia due to genetic mutations of cartilage matrix components, etc. even in the absence of mechanical stress, they are inadequate to study the mechanism of the stress-induced OA. Based on the hypothesis that the difficulty in elucidation of the OA mechanism is at least partly because the stress-induced OA animal

*Address correspondence and reprint requests to: Hiroshi Kawaguchi, Department of Orthopaedic Surgery, Faculty of Medicine, University of Tokyo, Hongo 7-3-1, Bunkyo, Tokyo 113-8655, Japan. Tel: 81-3-3815-5411x33376; Fax: 81-3-3818-4082; E-mail: kawaguchi-ort@h.u-tokyo.ac.jp

Received 10 August 2004; revision accepted 2 March 2005.

models have been confined to larger animals for which no gene manipulation technique has yet been developed, the present study aimed at creating stress-induced OA models in mice, that are reproducible and resemble the human OA, using a microsurgical technique to produce instability in the knee joints. The models were of four types: severe, moderate, mild, and medial, depending on the severity and direction of joint instability imposed by combinations of ligament transection and menisectomy. By combining these models, we performed histological analyses of the OA articular cartilage, and looked at the cellular and molecular changes in the development of OA.

Methods

EXPERIMENTAL ANIMALS AND SURGICAL PROCEDURES

All experiments were performed according to the protocol approved by the Animal Care and Use Committee of the University of Tokyo. C57Black6/J mice (18–22 g) were obtained from Charles River Japan Co. (Yokohama, Japan). Mice at 8 weeks of age were divided into three groups: severe, moderate, and mild models ($n = 30$/model). Under general anesthesia with pentobarbiturate (0.5 mg/10 g body weight, i.p., Sigma, St. Louis, Missouri), the bilateral hind limbs were shaved and prepared for aseptic surgery. Figure 1 summarizes the combinations of ligament transection and menisectomy in the mouse knee joints for the four models. In the severe model, the right knee joint was exposed and the patellar ligament (PL) was transected. Then, the anterior/posterior cruciate ligaments (ACL/PCL) and the medial/lateral collateral ligaments (MCL/LCL) were transected, and the medial/lateral menisci (MM/LM) were removed using a surgical microscope and microsurgical technique. After irrigation with saline to remove tissue debris, the skin incision was closed. During the procedure, close attention was paid not to injure the articular cartilage. The contralateral knee joint was sham-operated through the same approach without any ligament transection or menisectomy. The animals were allowed unrestricted activity, food, and water *ad libitum*. In the moderate model, the knee joint was exposed following a medial capsular incision and gentle lateral displacement of the extensor mechanism without transection of the PL. The ACL was transected and the MM was removed. After replacement of the extensor mechanism, the medial capsular incision was sutured and the skin was closed. In the mild model, using the same surgical approach as the moderate model, only ACL was transected and the incision was closed. The medial model was created without ACL transection; for this model the MCL was transected and the MM was removed through the same procedure ($n = 30$).

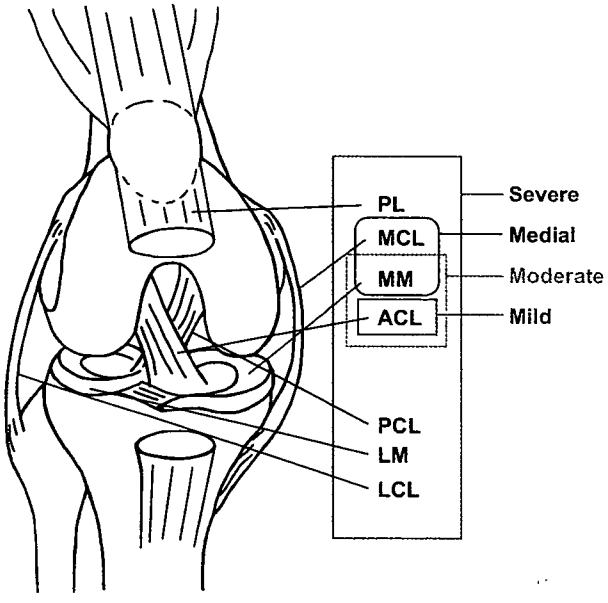

Fig. 1. Scheme of the mouse knee joint and the combinations of ligament transection and menisectomy in the severe, moderate, mild and medial models. PL, patellar ligament; MM, medial meniscus; LM, lateral meniscus; MCL, medial collateral ligament; LCL, lateral collateral ligament; ACL, anterior cruciate ligament; PCL, posterior cruciate ligament.

RADIOLOGICAL AND HISTOLOGICAL ANALYSES

Radiographs of the mouse knee joints were taken in the anteroposterior and lateral projections at 0 (immediately after surgery), 2, 4, and 8 weeks after surgery under general anesthesia using a soft X-ray apparatus (CMB-2; Softex Co., Tokyo, Japan), and were evaluated by a single observer who was blinded with regard to the experimental group. Mice of severe, moderate and mild models were sacrificed at 2, 4, and 8 weeks ($n = 10$ at each time point), and those of the medial model were sacrificed at 2, 4, 8 ($n = 7$ at each time point) and 12 weeks ($n = 9$). The numbers of mice were confirmed to be enough to perform statistical analyses[12]. The whole knee joints were dissected, and fixed in 4% paraformaldehyde (PFA) buffered with phosphate buffered saline (PBS) (pH 7.4) for 4 h at 4°C. The specimens were decalcified for 2 weeks with 10% ethylene-diamine tetraacetic acid (EDTA) (pH 7.4) at 4°C. After dehydration with an increasing concentration of ethanol and embedding in paraffin, 4 μm sagittal sections for the severe, moderate and mild models were cut from the whole medial compartment of the joints, and frontal sections for the medial model were cut from the whole joints. Sections were stained with Safranin-O-fast green, and the OA development in the tibial plateau was quantified by our original histological grading scores of 0–4 for cartilage destruction and 0–3 for osteophyte formation (Table I). The grade of OA was determined as the most advanced grade in all sections by a single observer who was blinded with regard to the experimental group. In an effort to control the inherent subjectivity of the assessment technique, all sections were graded by the same observer on two separate occasions, more than a month apart. Although the intraobserver reproducibility was confirmed to be more

Table I
Histological grading for osteoarthritic changes in mouse model

	Grade
I. Cartilage destruction	
A. No apparent changes	0
B. Loss of superficial zone in articular cartilage	1
C. Defects limited above tidemark	2
D. Defects extending to calcified cartilage	3
E. Exposure of subchondral bone	4
II. Osteophyte formation	
A. None	0
B. Formation of cartilage-like tissues	1
C. Increase of cartilaginous matrix	2
D. Endochondral ossification	3

than 90%, the mean value of the two scorings was defined as the final grade.

IMMUNOHISTOCHEMISTRY

Immunohistochemical localizations of type II, IX and X collagens, matrix metalloproteinase (MMP)-2, -3, -9 and -13 were performed in dewaxed paraffin sections as previously described[13]. The sections were treated with 0.3% hydrogen peroxide in PBS for 30 min at room temperature. To enhance the permeability of the extracellular matrix, glycosaminoglycans were removed by incubating the sections with 2.5% hyaluronidase (Sigma, St. Louis, Missouri) for 30 min at 37°C, as previously reported[14]. After blocking by PBS containing 1% bovine serum albumin (Sigma) for 1 h at room temperature, they were incubated with polyclonal rabbit antibodies against rat type II, IX and X collagens (LSL, Tokyo), and polyclonal goat antibodies against rabbit MMP-2, -3, -9 and -13 (CHEMICON International, Inc., Temecula, CA) at a dilution of 1:100 for 24 h at 4°C. As negative controls, we used non-immune rabbit or goat IgG of the same dilution instead of the primary antibodies. The sections were rinsed in PBS and incubated with the horseradish peroxidase (HRP)-conjugated goat antibodies against rabbit IgG (ICN Biomedicals, Inc., Aurora, Ohio) for 20 min at room temperature. The sections were washed with PBS, immersed in a diaminobenzidine solution for 10 min at room temperature to visualize any immunoreactivity, and were then counterstained with methylgreen.

IN SITU HYBRIDIZATION

In situ hybridization (ISH) with non-radioactive or radioactive probes was performed as previously described with minor modifications[15]. In brief, dewaxed paraffin sections were postfixed with 4% PFA buffered with PBS (PFA–PBS) for 15 min at room temperature. After washing with PBS, sections were digested with 10 μg/ml proteinase K for 15 min in PBS, treated again with 4% PFA–PBS for 10 min to inactivate proteinase K, washed with PBS, incubated with 0.2 N HCl for 10 min, washed with PBS, acetylated with 0.3% acetic anhydride in the presence of 0.1 M triethanolamine for 10 min, treated with 3% hydrogen peroxide/methanol for 30 min, dehydrated with increasing concentrations of ethanol, and air dried. Hybridization with complementary digoxigenin (DIG)-labeled or ^{35}S-labeled riboprobes for mouse *type X collagen* (generously given by B. Olsen, Harvard Medical School, Boston, MA) and mouse *MMP-13* (generously given by S. Schipani, Massachusetts General Hospital, Boston) was performed in a humidified chamber in a solution containing 50% formamide, 10% dextran sulfate, 1× Denhardt's solution, 600 mM NaCl, 10 mM dithiothreitol, 0.25% sodium dodecyl sulfate, and 150 μg/ml transfer RNA for 16 h at 52°C. After hybridization, sections were sequentially washed once with 50% formamide/2× saline sodium citrate (SSC) for 5 min at 52°C, twice with 2× SSC for 1 min at room temperature, once with 10 μg/ml RNaseA/2× SSC for 30 min at 37°C, twice with 2× SSC for 1 min at room temperature, and once with 50% formamide/2× SSC for 5 min at 52°C. For the detection of DIG-labeled probes, slides were blocked by PBS containing 1% bovine serum albumin (Sigma) for 10 min at room temperature, and incubated with HRP-conjugated anti-DIG rabbit polyclonal antibody (Dakopatts, Glostrup, Denmark) at a dilution of 1:100 for 24 h at 4°C. After washing three times with tris-buffered saline containing 0.1% Tween-20 (TBS-T), the sections were immersed in a diaminobenzidine solution for 10 min at room temperature to visualize immunoreactivity, then were counterstained with methylgreen. For the detection of radioactive probes, slides were placed on X-ray films, and the autoradiographs were obtained after overnight exposure. Slides were dipped into NTB-2 (Eastman Kodak, New Haven, CT) and stored at 4°C for the times estimated from the intensity of signals on the X-ray film. After development, sections were counterstained with hematoxylin–eosin.

STATISTICAL ANALYSIS

Means of groups were compared by ANOVA and significance of differences was determined by *post-hoc* testing with Bonferroni's method.

Results

TIME COURSE OF RADIOLOGICAL CHANGES IN THE SEVERE, MODERATE AND MILD MODELS

We first performed radiological analyses of the knee joints in the severe, moderate and mild models (Fig. 2). All mice in the three models exhibited anterior subluxation of the tibiae causing joint destruction and osteophyte formation at the posterior part of the joints. The progression speed of the radiological disorders was dependent upon the severity of joint instability induced by the surgery. The severe model showed joint destruction at 2 weeks and osteophyte formation at the posterior tibiae 4 weeks after surgery. The moderate model showed joint destruction and osteophyte formation at 4 weeks, both of which progressed thereafter. Contrarily in the mild model these changes could not be detected until 8 weeks, although the deterioration of joint congruency and the subchondral sclerotic changes were visible at 8 weeks.

TIME COURSE OF HISTOLOGICAL CHANGES IN THE SEVERE, MODERATE AND MILD MODELS

Histological examinations were then made using Safranin-O staining to learn more of the time course of OA development. In the sham-operated knee joints of the contralateral side, the articular cartilage of the tibiae had a smooth surface, evenly stained with Safranin-O, and attached to the subchondral bone 8 weeks after surgery [Fig. 3(A)]. In the superficial zone of the tibial articular cartilage, one or two layers of flat cells were arranged tangentially, and round cells were observed in the middle zone above the tidemark. These histological findings were similar to those of normal knee cartilage of mice without any surgical intervention at the same age.

Figure 3(B) shows low (left panel) and high (right panel) magnifications of joints, which principally demonstrate the osteophyte formation and cartilage destruction, respectively, at the posterior tibiae in severe, moderate and mild models. In the low magnification feature of the severe model, a cartilaginous tissue extended from the posterior tibial cartilage 2 weeks after surgery, and gradually grew with an increase of the Safranin-O staining at 4 weeks. By 8 weeks, the tissue had developed into an osteophyte through endochondral ossification. In the moderate model, the maturation and development of osteophyte were somewhat slower, corresponding to the radiological findings. Contrarily, osteophyte formation was hardly visible in the mild model until 8 weeks. In these three models,

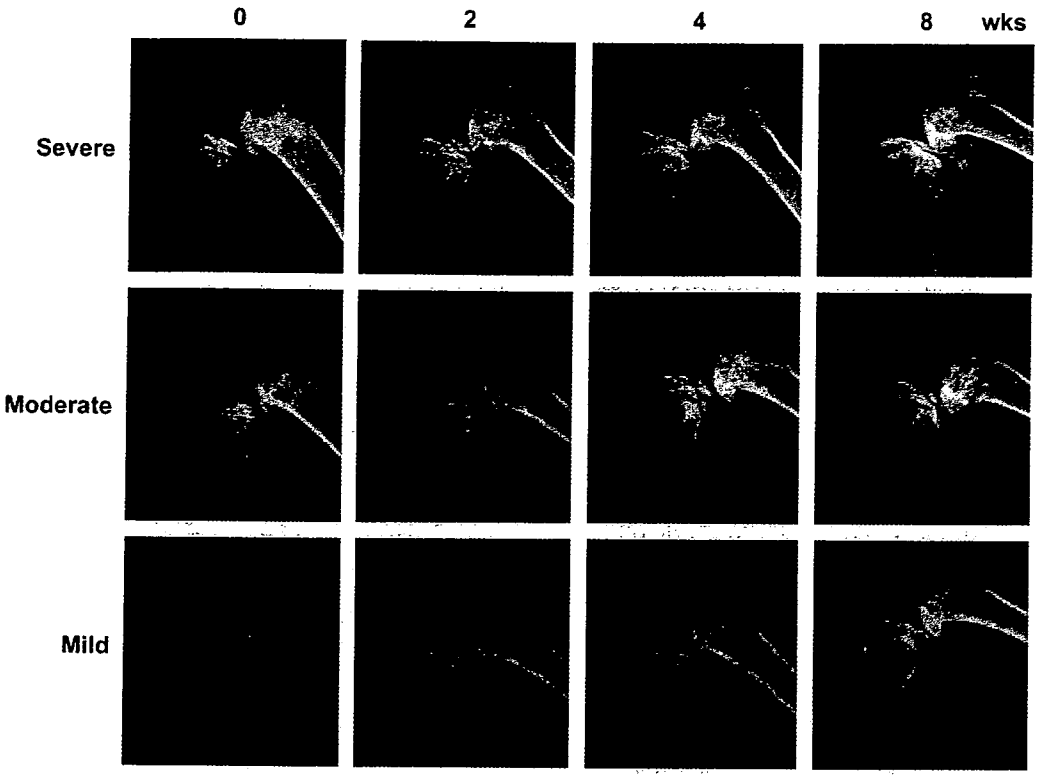

Fig. 2. Time course of lateral X-ray features of the knee joints in the severe, moderate and mild models. Radiographs were taken at the indicated weeks after surgery under general anesthesia using a soft X-ray apparatus. Due to the anterior subluxation of the tibiae, joint destruction and osteophyte formation were visible in the posterior tibial plateau. The changes were dependent on the time after surgery and the severity of joint instability.

thickened synovium due to inflammatory reaction to the surgical invasion was visible at 2 weeks, but not thereafter.

The cartilage destruction at the tibiae seen in the high magnification features of the severe model showed a loss of the superficial zone, a decrease in Safranin-O staining and an increase in cellularity in the middle zone at 2 weeks. At 4 weeks, the defect of the articular cartilage had developed into the calcified cartilage layer below the tidemark, and finally almost the full thickness of the articular cartilage was destroyed by 8 weeks. In the moderate model, the early stage disorders were also noted within 2 weeks, while the defect of articular cartilage was limited to the area above the tidemark at 4 weeks, and gradually extended to the calcified cartilage at 8 weeks. The mild model did not exhibit any changes in the articular cartilage at 2 weeks, but proliferation and shape change of chondrocytes began by 4 weeks. Cartilage destruction in the mild model rarely reached the middle layer even at 8 weeks.

In order to quantify the time course of OA development in the three models, we used our original gradings for cartilage destruction and osteophyte formation (Table I). For the grading of the cartilage destruction, we referred to the simple scoring systems in mouse OA models by Wilhelmi and Faust[10], Helminen *et al.*[16], Chambers *et al.*[17], Saamanen *et al.*[11], and Price *et al.*[18], and modified them, because the mouse cartilage contains only a few cell layers. In addition, osteophyte formation was graded into four ranks, according to the process of endochondral ossification. Based on the histological grading scores, both cartilage destruction and osteophyte formation increased as functions of time after surgery and severity of joint instability (Fig. 4). The severe model exhibited the most drastic increases of both parameters, while the moderate model showed somewhat lower scores, although not significantly different from the severe model. The scores of the mild model were the lowest and remained less than half those of the other two models throughout the observation period up to 8 weeks.

TIME COURSE OF HISTOLOGICAL CHANGES IN THE MEDIAL MODEL

Since the three models above include the ACL transection, they exhibited the anterior subluxation causing the OA development at the posterior part of the joints. Considering that most of the clinical knee OA cases have major disorders in the medial tibial cartilage, we performed transection of the MCL instead of the ACL. Although the MCL transection alone did not lead to any OA changes until 12 weeks after surgery (data not shown), the combination of MCL transection and medial menisectomy caused the cartilage destruction and osteophyte formation in the medial tibial cartilage (Fig. 5). The time course of OA development was similar to or slightly more severe than that of the mild model: proliferation and shape change of chondrocytes at 2–4 weeks, cartilage destruction into the middle zone at 8 weeks, and osteophyte formation at 12 weeks.

COLLAGEN AND MMP EXPRESSION IN THE MOUSE OA MODELS

Cellular changes in the early stage of OA cartilage were determined by immunohistochemistry and ISH for collagens and MMPs, both of which have been implicated in OA

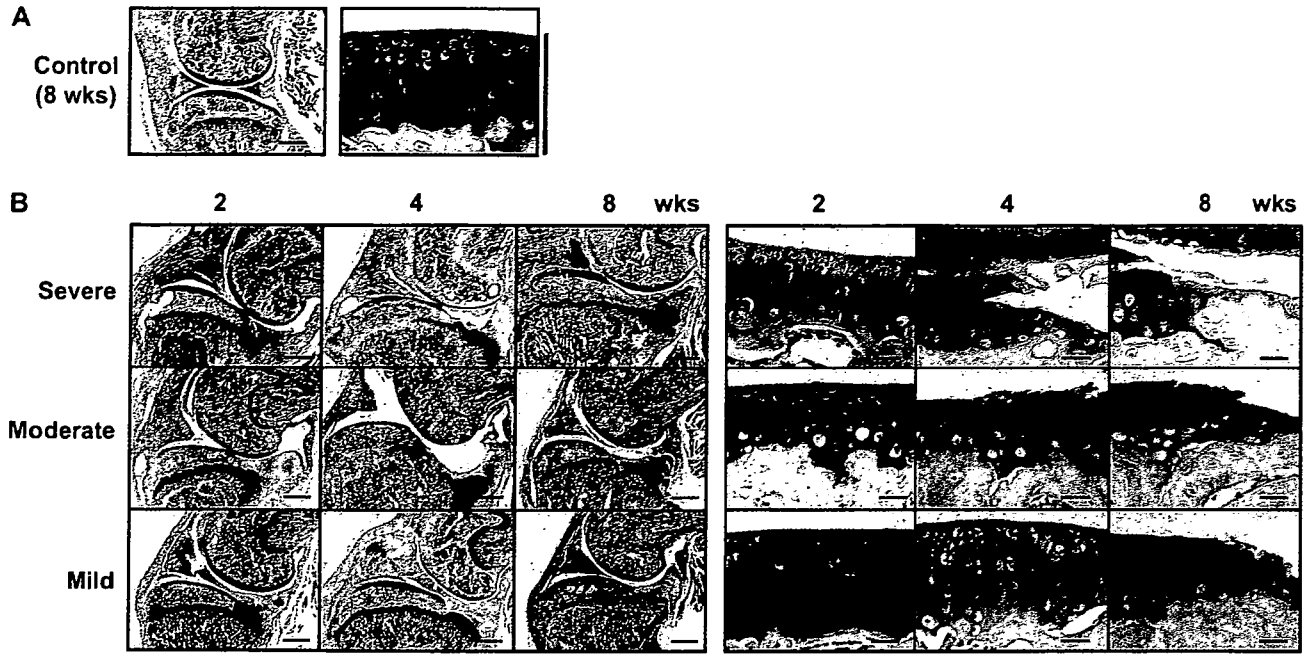

Fig. 3. Time course of histology of the knee joints in the severe, moderate and mild models. After fixation, decalcification and embedding, 4 μm sagittal sections were cut from the whole knee joints, and were stained with Safranin-O-fast green. Arrowheads indicate the level of the tide mark. Scale bar, 1 mm and 50 μm for low and high magnifications, respectively. (A) Low (left) and high (right) magnifications of sham-operated knee joints 8 weeks after surgery. Blue, red, green, and black bars indicate superficial zone, middle/deep zones, calcified cartilage, and subchondral bone, respectively. (B) Low (left) and high (right) magnifications of severe, moderate and mild models at the indicated weeks after surgery, which represent osteophyte formation and cartilage destruction, respectively.

development. The immunohistochemical localization of cartilage specific type II and IX collagens was comparable between the OA cartilage in the moderate model and the sham-operated control 2 weeks after surgery [Fig. 6(A)]. In both mice, type II collagen was strongly stained in all zones of the articular cartilage both above and below the tidemark, while type IX collagen was mainly localized in and around chondrocytes in the superficial and middle zones of cartilage above the tidemark, but weakly in the calcified cartilage below the tidemark. Type X collagen, a specific marker of hypertrophic chondrocytes, was faintly stained in the calcified cartilage below the tidemark; however, the OA cartilage showed its immunoreactivity in and around chondrocytes above the tidemark. ISH confirmed the expression of mRNA in chondrocytes of these areas, indicating the presence of pathological chondrocytes that undergo hypertrophic differentiation in the early stage of OA development [Fig. 6(B)]. In the severe, mild, and medial models, type X collagen expression in chondrocytes of the superficial and middle zones was also seen at 1, 4, and 4 weeks, respectively, after surgery (data not shown).

We next compared MMP-2, -3, -9 and -13 expression between the OA cartilage in the moderate model and the sham-operated control 2 weeks after surgery [Fig. 7(A)].

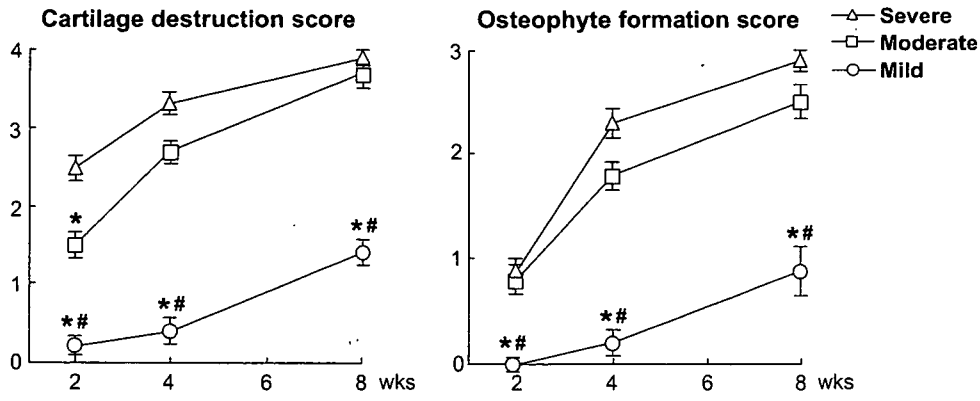

Fig. 4. Time course of OA development by the histological grading scores in the severe, moderate and mild models. The OA development was graded by scores of 0–4 for cartilage destruction and 0–3 for osteophyte formation as shown in Table I. Both cartilage destruction and osteophyte formation scores increased as functions of time after surgery and severity of joint instability. Data are expressed as the means (symbols) ± S.E.M. (error bars) for 10 mice/time point in each model. *$P < 0.01$ vs severe model, #$P < 0.01$ vs moderate model.

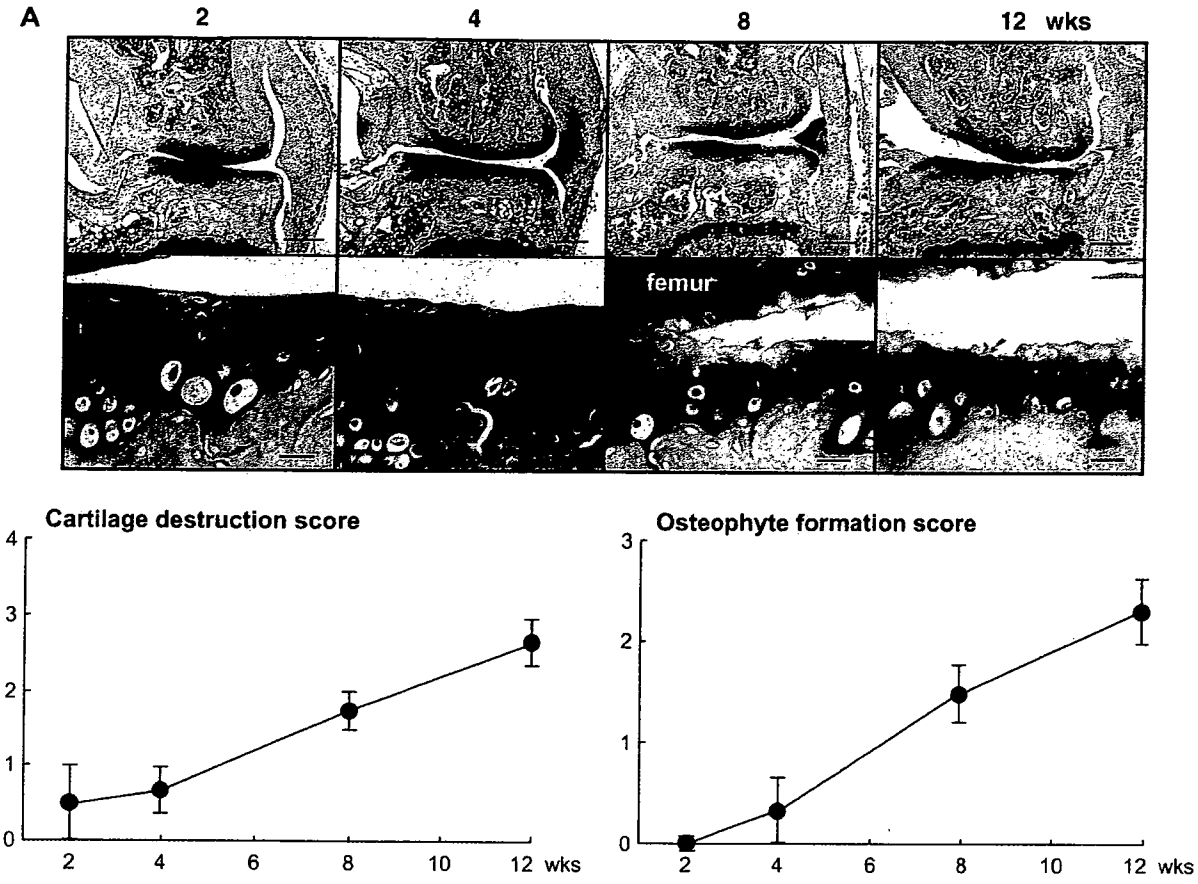

Fig. 5. Time course of OA development in the medial model. After fixation, decalcification and embedding, 4 μm frontal sections were cut from the whole knee joints, and were stained with Safranin-O-fast green. (A) Histological features of low (top) and high (bottom) magnifications at the indicated weeks after surgery. Arrowheads indicate the level of the tide mark. Scale bar, 500 μm and 50 μm for low and high magnifications, respectively. (B) Time course of OA development by the histological grading as shown in Table I. Data are expressed as the means (symbols) ± S.E.M. (error bars) for seven mice at 2, 4, 6 weeks and for nine mice at 12 weeks.

MMP-2 and MMP-9 were localized solely in the calcified cartilage and subchondral bone area, while MMP-3 immunolocalization was visible above the tidemark. These localizations were similar in the OA and control cartilages. In contrast, the immunostaining of MMP-13 was enhanced in the superficial and middle zones of the OA cartilage, which was rarely seen in the control. Since the localization of MMP-13 was quite similar to that of type X collagen shown in Fig. 6(A), we assume that MMP-13 is produced by pathological hypertrophic chondrocytes in early OA cartilage.

To examine the expression patterns of type X collagen and MMP-13 in more advanced OA cartilage, immunostaining was performed in the severe model 4 weeks after surgery. These were also colocalized in the areas adjacent to the destructive lesion of the OA cartilage, confirming the close connection between the hypertrophic differentiation and MMP-13 production by chondrocytes [Fig. 7(B), top]. When ISH analyses of type X collagen and MMP-13 in the growth plate of fetal mouse tibiae (E17.5) were performed to examine their connection under physiological conditions, they were not colocalized as in OA cartilage: only the highly differentiated cells in the type X collagen-positive chondrocytes expressed MMP-13. These results suggest that the appearance of abnormal chondrocytes that simultaneously undergo hypertrophic differentiation and MMP-13 expression in the superficial and middle zones is characteristic in the development of OA.

Discussion

As a first step in applying mouse genomics that has recently made a breakthrough in the biological research on OA development, the present study established four types of experimental mouse OA models by producing instability in the knee joints. Although it may seem difficult to perform the operation in the small joints of mice without direct damage at the time of surgery, microscopic and microsurgical technique have made it much safer and easier. In fact, a beginner performing the operation for the first time who has at least experience in clinical surgery under a microscope can accomplish the entire procedure within 20 min without damaging the articular cartilage.

The early stage changes in the mouse articular cartilage after surgery were found to be a defect of the superficial zone and a decrease of Safranin-O staining, followed by progressing cartilage destruction and aggravation of joint congruency that created a vicious circle to advance the condition. These changes were identical to the human OA pathology reported as arthroscopic and histological findings[19,20]. Along with the catabolic changes, anabolic reactions such as chondrocyte proliferation, subchondral sclerosis, and osteophyte formation were also seen in the human OA cartilage. Although previous OA models of larger animals are known to recapitulate these anabolic changes[7], it was difficult to accurately evaluate and quantify the

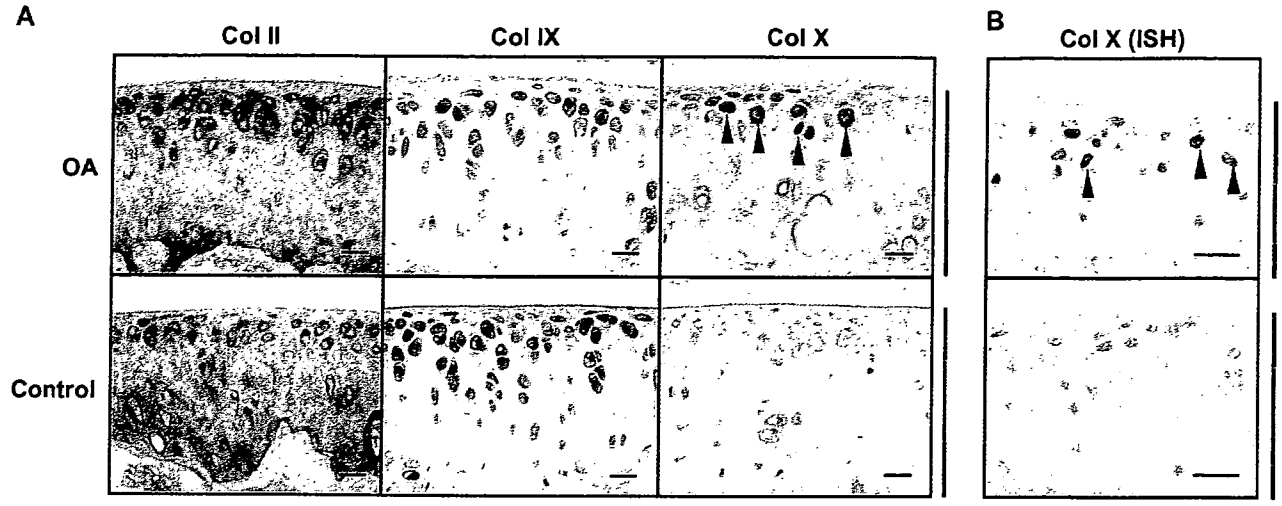

Fig. 6. Immunohistochemistry for type II, IX and X collagens (Col II, Col IX and Col X) (A) and ISH for Col X mRNA (B) in the OA and control cartilages. Stainings of the OA cartilage in the moderate model and the sham-operated control 2 weeks after surgery. Blue, red, green, and black bars indicate superficial zone, middle/deep zones, calcified cartilage, and subchondral bone, respectively. Scale bar, 50 μm. Immunohistochemistry was performed in dewaxed paraffin sections with polyclonal rabbit antibodies against rat Col II, Col IX and Col X as described in Methods. ISH was performed in the paraffin sections using complementary DIG-labeled riboprobes for mouse Col X. The sections were counterstained with methylgreen. Although Col II and Col IX expressions were similar between the OA and control cartilages, Col X was localized in the chondrocytes of the superficial and middle zones (arrowheads) of the OA cartilage, but not of the control.

chondrocyte proliferation and subchondral bone sclerosis in the current mouse models in which the articular cartilage contains only a few cell layers. We therefore did not include the anabolic parameters except the osteophyte formation in the present histological grading system, and created a simpler system than Mankin's grading system[21] that is frequently used for OA of larger animals and humans.

Although the instability was present in the knee joints, the OA change was much more severe in the tibial cartilage than in the femoral condyle cartilage. Since the cartilage layer is much thinner and osteophyte formation is rarely seen in the femoral condyle, it is difficult to quantify OA development with the same accuracy as in the tibial cartilage. Hence, the current models focused on OA change in the tibial cartilage. In the three models with ACL transection, severe, moderate and mild, OA development in the posterior tibial cartilage was dependent on the severity of joint instability, indicating that combinations of these models will enable us to identify the molecular backgrounds at various stages. The severe and moderate models appeared to be useful to evaluate reactive osseous changes like osteophyte formation which is characteristic in the late stage of OA. Because the moderate model showed somewhat slower progress in the early stage of cartilage destruction than the severe model, this model also seemed suitable to follow the entire process including the early stage changes. The OA development in the mild model was limited to a partial cartilage destruction, and chondrocyte morphology was relatively preserved during the observation period, indicating that this model is useful for detailed investigations of the early stage.

There is a recent report using a mouse OA model through MCL transection and partial medial menisectomy of the knee joints[22]. In that study, Clements *et al.* observed OA development in mice lacking interleukin-1β (IL-1β), IL-1β-converting enzyme, stromelysin 1 or inducible nitric oxide synthase, all of which were theoretically thought to play important roles in the development of the condition[23]. However, all mutant mice unexpectedly exhibited an acceleration of cartilage destruction 4 weeks after surgery, implying that these factors were essential for balancing anabolism and catabolism in the early stage of OA development, as the authors discussed. The Clements model resembles the medial model in the present study, which showed OA development in the medial compartment of the joint just like most cases of human knee OA. Although OA progression in the medial model was similar to or slightly more rapid than that in the posterior cartilage of the mild model, late stage changes including osteophyte formation could be observed. The differences between the Clements model and our medial model are the range of menisectomy and the observation period: partial (about half) menisectomy and 4-week observation for the former, and total menisectomy and 12-week observation for the latter. Creating our medial model in the mutant mice will enable us to examine the effects of these catabolic factors on the OA development not only in the early stage, but also in the later stages, which might be differently regulated. Furthermore, application of combinations of three types of models with ACL transection will elucidate the stage-specific role of the factors in more detail.

The usefulness of the models was demonstrated by immunohistochemistry and ISH of collagens and MMPs, showing that type X collagen and MMP-13 were induced and colocalized in OA cartilage. Articular cartilage is considered to be a permanent cartilage that is free from hypertrophic chondrocytes with type X collagen expression except for the calcified cartilage. In fact, type X collagen localization in the sham-operated knee cartilage was limited to the area below the tidemark; however, in the OA cartilage, type X collagen was strongly expressed in chondrocytes above the tidemark. Previous studies supported the increase in the expression of type X collagen in OA articular chondrocytes, and some reports showed that other ectopic terminal differentiation markers including annexin VI, alkaline phosphatase, osteopontin, and osteocalcin were detected in the OA chondrocytes[24–27]. In the meantime, the expression of MMP-13 that potently degrades cartilage matrix with preference to type II collagen is reported to be upregulated in OA[28,29]. The

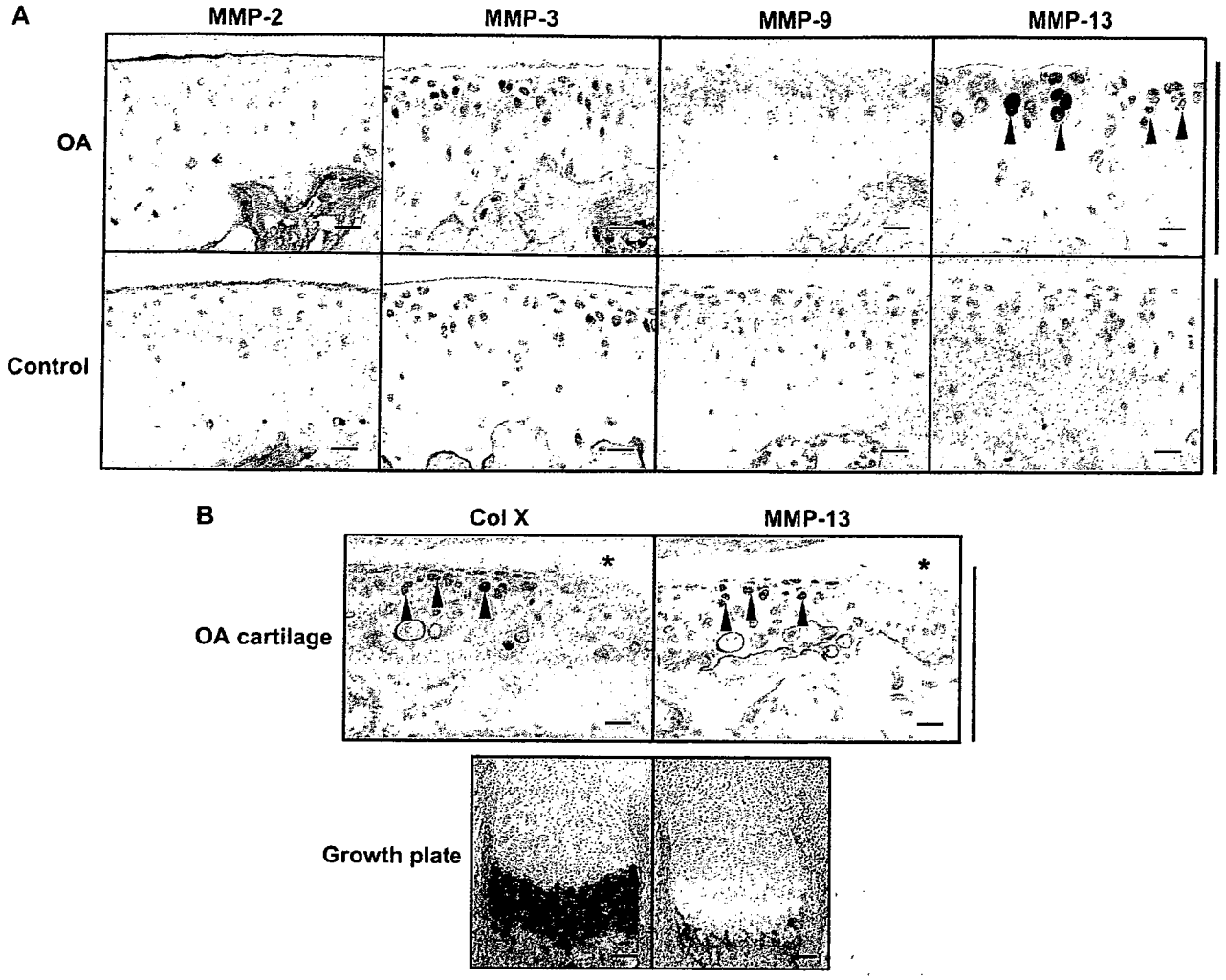

Fig. 7. Immunohistochemistry for MMP-2, -3, -9 and -13 in the OA and control cartilages (A), and the localizations of type X collagen (Col X) and MMP-13 in the OA cartilage and the growth plate (B). Blue, red, green, and black bars indicate superficial zone, middle/deep zones, calcified cartilage, and subchondral bone, respectively. (A) Immunostainings of the OA cartilage in the moderate model and the sham-operated control 2 weeks after surgery. Immunohistochemistry was performed in dewaxed paraffin sections with polyclonal goat antibodies against rabbit MMP-2, -3, -9 and -13 as described in Methods. The sections were counterstained with methylgreen. Scale bar, 50 μm. (B) Top: Immunostainings for Col X and MMP-13 of the OA cartilage in the severe model 4 weeks after surgery. Bottom: ISH for Col X and MMP-13 in the tibial growth plate of mouse embryo (E17.5). In the OA cartilage MMP-13 and Col X (arrowheads) were colocalized in the vicinity of the defect lesion (asterisk), although in the normal growth plate only the highly differentiated subpopulation in the Col X-positive chondrocytes expressed MMP-13. Scale bar, 100 μm.

transgenic mouse expressing constitutively active MMP-13 showed OA changes under physiological conditions[30], suggesting a close relationship between MMP-13 and cartilage destruction in OA. These findings suggest that articular chondrocytes could not maintain characters of a permanent cartilage during OA development, but gained those of a differentiating cartilage such as growth plate and fracture callus. The previous and present studies revealed that in the growth plate there is a strict regulation between type X collagen and MMP-13 expression patterns: only the highly differentiated cells in the type X collagen-positive chondrocytes expressed MMP-13[31,32]. This sequence of expression may be important for the physiological process of endochondral ossification following the cartilage matrix degradation during skeletal growth. However, in OA cartilage, this hierarchy was disrupted: MMP-13 expression was colocalized with that of type X collagen in chondrocytes above the tidemark. We thus speculate that recruitment of abnormal chondrocytes that simultaneously undergo hypertrophic differentiation and MMP-13 expression under the stimulation of mechanical stress may be a key event in the development of OA.

In summary, we established four types of mouse models exhibiting various speeds of OA progression stimulated by mechanical stress. These models were practical, reproducible, and showed pathologic features similar to human OA. And, more importantly, by applying a mouse genomics approach to the models, molecular backgrounds in various stages of OA development could be examined. Hence, the next task will be to apply the models to mice lacking or overexpressing candidate genes. First, we are interested in the OA development in MMP-13-deficient mice. In addition, chondrocyte hypertrophy and MMP-13 remind us of a transcriptional activator Runx2 that is known to positively regulate both of them[33–39]. Although homozygous Runx2-deficient mice died just after birth, the heterozygous

deficient mice developed and grew normally without abnormalities of major organs except for cleidocranial dysplasia[33,40]. Studies creating OA models in these deficient mice are now underway.

References

1. Doherty M. Risk factors for progression of knee osteoarthritis. Lancet 2001;358:775–6.
2. Haywood L, McWilliams DF, Pearson CI, Gill SE, Ganesan A, Wilson D, *et al.* Inflammation and angiogenesis in osteoarthritis. Arthritis Rheum 2003; 48:2173–7.
3. Mollenhauer JA, Erdmann S. Introduction: molecular and biomechanical basis of osteoarthritis. Cell Mol Life Sci 2002;59:3–4.
4. Haq I, Murphy E, Dacre J. Osteoarthritis. Postgrad Med J 2003;79:377–83.
5. Brandt KD. Animal models: insights into osteoarthritis (OA) provided by the cruciate-deficient dog. Br J Rheumatol 1991;30(Suppl 1):5–9.
6. Brandt KD. Animal models of osteoarthritis. Biorheology 2002;39:221–35.
7. Bendele AM. Animal models of osteoarthritis. J Musculoskelet Neuron Interact 2001;1:363–76.
8. Hayami T, Pickarski M, Wesolowski GA, McLane J, Bone A, Destefano J, *et al.* The role of subchondral bone remodeling in osteoarthritis: reduction of cartilage degeneration and prevention of osteophyte formation by alendronate in the rat anterior cruciate ligament transection model. Arthritis Rheum 2004;50: 1193–206.
9. Walton M. Patella displacement and osteoarthrosis of the knee joint in mice. J Pathol 1979;127:165–72.
10. Wilhelmi G, Faust R. Suitability of the C57 black mouse as an experimental animal for the study of skeletal changes due to ageing, with special reference to osteo-arthrosis and its response to tribenoside. Pharmacology 1976;14:289–96.
11. Saamanen AK, Salminen HJ, Dean PB, De Crombrugghe B, Vuorio EI, Metsaranta MP. Osteoarthritis-like lesions in transgenic mice harboring a small deletion mutation in type II collagen gene. Osteoarthritis Cartilage 2000;8:248–57.
12. Dell RB, Holleran S, Ramakrishnan R. Sample size determination. ILAR J 2002;43:207–13.
13. Hoshi K, Komori T, Ozawa H. Morphological characterization of skeletal cells in Cbfa1-deficient mice. Bone 1999;25:639–51.
14. Stoop R, Buma P, van der Kraan PM, Hollander AP, Clark Billinghurst R, Robin Poole A, *et al.* Differences in type II collagen degradation between peripheral and central cartilage of rat stifle joints after cranial cruciate ligament transection. Arthritis Rheum 2000;43: 2121–31.
15. Lee K, Deeds JD, Segre GV. Expression of parathyroid hormone-related peptide and its receptor messenger ribonucleic acids during fetal development of rats. Endocrinology 1995;136:453–63.
16. Helminen HJ, Kiraly K, Pelttari A, Tammi MI, Vandenberg P, Pereira R, *et al.* An inbred line of transgenic mice expressing an internally deleted gene for type II procollagen (COL2A1). Young mice have a variable phenotype of a chondrodysplasia and older mice have osteoarthritic changes in joints. J Clin Invest 1993;92: 582–95.
17. Chambers MG, Bayliss MT, Mason RM. Chondrocyte cytokine and growth factor expression in murine osteoarthritis. Osteoarthritis Cartilage 1997;5: 301–8.
18. Price JS, Chambers MG, Poole AR, Fradin A, Mason RM. Comparison of collagenase-cleaved articular cartilage collagen in mice in the naturally occurring STR/ort model of osteoarthritis and in collagen-induced arthritis. Osteoarthritis Cartilage 2002;10:172–9.
19. Poole AR. An introduction to the pathophysiology of osteoarthritis. Front Biosci 1999;4:D662–70.
20. Santori N, Villar RN. Arthroscopic findings in the initial stages of hip osteoarthritis. Orthopedics 1999;22: 405–9.
21. Mankin HJ, Johnson ME, Lippiello L. Biochemical and metabolic abnormalities in articular cartilage from osteoarthritic human hips. III. Distribution and metabolism of amino sugar-containing macromolecules. J Bone Joint Surg Am 1981;63:131–9.
22. Clements KM, Price JS, Chambers MG, Visco DM, Poole AR, Mason RM. Gene deletion of either interleukin-1beta, interleukin-1beta-converting enzyme, inducible nitric oxide synthase, or stromelysin 1 accelerates the development of knee osteoarthritis in mice after surgical transection of the medial collateral ligament and partial medial meniscectomy. Arthritis Rheum 2003;48:3452–63.
23. Poole AR, Howell DS. Etiopathies of osteoarthritis. In: Moskowitz RW, Howell DS, Altman RD, Buckwalter JA, Goldberg VM, Eds. Osteoarthritis: Diagnosis and Medical/Surgical Management. Philadelphia: Saunders 2001;29–47.
24. von der Mark K, Kirsch T, Nerlich A, Kuss A, Weseloh G, Gluckert K, *et al.* Type X collagen synthesis in human osteoarthritic cartilage. Indication of chondrocyte hypertrophy. Arthritis Rheum 1992; 35:806–11.
25. Boos N, Nerlich AG, Wiest I, von der Mark K, Ganz R, Aebi M. Immunohistochemical analysis of type-X-collagen expression in osteoarthritis of the hip joint. J Orthop Res 1999;17:495–502.
26. Pullig O, Weseloh G, Gauer S, Swoboda B. Osteopontin is expressed by adult human osteoarthritic chondrocytes: protein and mRNA analysis of normal and osteoarthritic cartilage. Matrix Biol 2000;19: 245–55.
27. Pfander D, Swoboda B, Kirsch T. Expression of early and late differentiation markers (proliferating cell nuclear antigen, syndecan-3, annexin VI, and alkaline phosphatase) by human osteoarthritic chondrocytes. Am J Pathol 2001;159:1777–83.
28. Mitchell PG, Magna HA, Reeves LM, Lopresti-Morrow LL, Yocum SA, Rosner PJ, *et al.* Cloning, expression, and type II collagenolytic activity of matrix metalloproteinase-13 from human osteoarthritic cartilage. J Clin Invest 1996;97:761–8.
29. Billinghurst RC, Dahlberg L, Ionescu M, Reiner A, Bourne R, Rorabeck C, *et al.* Enhanced cleavage of type II collagen by collagenases in osteoarthritic articular cartilage. J Clin Invest 1997;99:1534–45.
30. Neuhold LA, Killar L, Zhao W, Sung ML, Warner L, Kulik J, *et al.* Postnatal expression in hyaline cartilage of constitutively active human collagenase-3 (MMP-13) induces osteoarthritis in mice. J Clin Invest 2001;107:35–44.

31. D'Angelo M, Yan Z, Nooreyazdan M, Pacifici M, Sarment DS, Billings PC, *et al.* MMP-13 is induced during chondrocyte hypertrophy. J Cell Biochem 2000; 77:678–93.
32. Jimenez MJ, Balbin M, Alvarez J, Komori T, Bianco P, Holmbeck K, *et al.* A regulatory cascade involving retinoic acid, Cbfa1, and matrix metalloproteinases is coupled to the development of a process of perichondrial invasion and osteogenic differentiation during bone formation. J Cell Biol 2001;155:1333–44.
33. Komori T, Yagi H, Nomura S, Yamaguchi A, Sasaki K, Deguchi K, *et al.* Targeted disruption of Cbfa1 results in a complete lack of bone formation owing to maturational arrest of osteoblasts. Cell 1997;89: 755–64.
34. Inada M, Yasui T, Nomura S, Miyake S, Deguchi K, Himeno M, *et al.* Maturational disturbance of chondrocytes in Cbfa1-deficient mice. Dev Dyn 1999;214: 279–90.
35. Jimenez MJ, Balbin M, Lopez JM, Alvarez J, Komori T, Lopez-Otin C. Collagenase 3 is a target of Cbfa1, a transcription factor of the runt gene family involved in bone formation. Mol Cell Biol 1999;19:4431–42.
36. Porte D, Tuckermann J, Becker M, Baumann B, Teurich S, Higgins T, *et al.* Both AP-1 and Cbfa1-like factors are required for the induction of interstitial collagenase by parathyroid hormone. Oncogene 1999; 18:667–78.
37. Ueta C, Iwamoto M, Kanatani N, Yoshida C, Liu Y, Enomoto-Iwamoto M, *et al.* Skeletal malformations caused by overexpression of Cbfa1 or its dominant negative form in chondrocytes. J Cell Biol 2001;153: 87–100.
38. Takeda S, Bonnamy JP, Owen MJ, Ducy P, Karsenty G. Continuous expression of Cbfa1 in nonhypertrophic chondrocytes uncovers its ability to induce hypertrophic chondrocyte differentiation and partially rescues Cbfa1-deficient mice. Genes Dev 2001;15:467–81.
39. Otto F, Lubbert M, Stock M. Upstream and downstream targets of RUNX proteins. J Cell Biochem 2003;89: 9–18.
40. Otto F, Thornell AP, Crompton T, Denzel A, Gilmour KC, Rosewell IR, *et al.* Cbfa1, a candidate gene for cleidocranial dysplasia syndrome, is essential for osteoblast differentiation and bone development. Cell 1997;89:765–71.

Suppression of Aging in Mice by the Hormone Klotho

Hiroshi Kurosu,[1] Masaya Yamamoto,[1] Jeremy D. Clark,[1] Johanne V. Pastor,[1] Animesh Nandi,[1] Prem Gurnani,[1] Owen P. McGuinness,[3] Hirotaka Chikuda,[4] Masayuki Yamaguchi,[4] Hiroshi Kawaguchi,[4] Iichiro Shimomura,[5] Yoshiharu Takayama,[2] Joachim Herz,[2] C. Ronald Kahn,[6] Kevin P. Rosenblatt,[1] Makoto Kuro-o[1]*

A defect in *Klotho* gene expression in mice accelerates the degeneration of multiple age-sensitive traits. Here, we show that overexpression of *Klotho* in mice extends life span. Klotho protein functions as a circulating hormone that binds to a cell-surface receptor and represses intracellular signals of insulin and insulin-like growth factor 1 (IGF1), an evolutionarily conserved mechanism for extending life span. Alleviation of aging-like phenotypes in Klotho-deficient mice was observed by perturbing insulin and IGF1 signaling, suggesting that Klotho-mediated inhibition of insulin and IGF1 signaling contributes to its anti-aging properties. Klotho protein may function as an anti-aging hormone in mammals.

Klotho was originally identified as a mutated gene in a mouse strain that accelerates age-dependent loss of function in multiple age-sensitive traits (*1*). An insertional mutation that disrupts the 5′ promoter region of the *Klotho* gene resulted in a strong hypomorphic allele. Mice homozygous for the mutated allele ($KL^{-/-}$ mice) appeared normal until 3 to 4 weeks old but then began to manifest multiple age-related disorders observed in humans, including ectopic calcification, skin atrophy, muscle atrophy, osteoporosis, arteriosclerosis, and pulmonary emphysema. $KL^{-/-}$ mice suffered premature death around two months of age.

The *Klotho* gene encodes a single-pass transmembrane protein that is detectable in limited tissues, particularly the distal convoluted tubules in the kidney and the choroid plexus in the brain. Because a defect in the *Klotho* gene leads to systemic age-dependent

[1]Department of Pathology, [2]Department of Molecular Genetics, University of Texas (UT) Southwestern Medical Center at Dallas, 5323 Harry Hines Boulevard, Dallas, TX 75390–9072, USA. [3]Department of Molecular Physiology and Biophysics, Vanderbilt University School of Medicine, 702 Light Hall, Nashville, Tennessee 37232–0615, USA. [4]Department of Sensory and Motor System Medicine, University of Tokyo, 7-3-1 Hongo, Bunkyo, Tokyo 113-8655, Japan. [5]Department of Internal Medicine and Molecular Science, Graduate School of Medicine, Osaka University, 2-2 Yamadaoka, Suita, Osaka 565-0871, Japan. [6]Research Division, Joslin Diabetes Center, Department of Medicine, Harvard Medical School, One Joslin Place, Boston, MA 02215, USA.

*To whom correspondence should be addressed. E-mail: makoto.kuro-o@utsouthwestern.edu

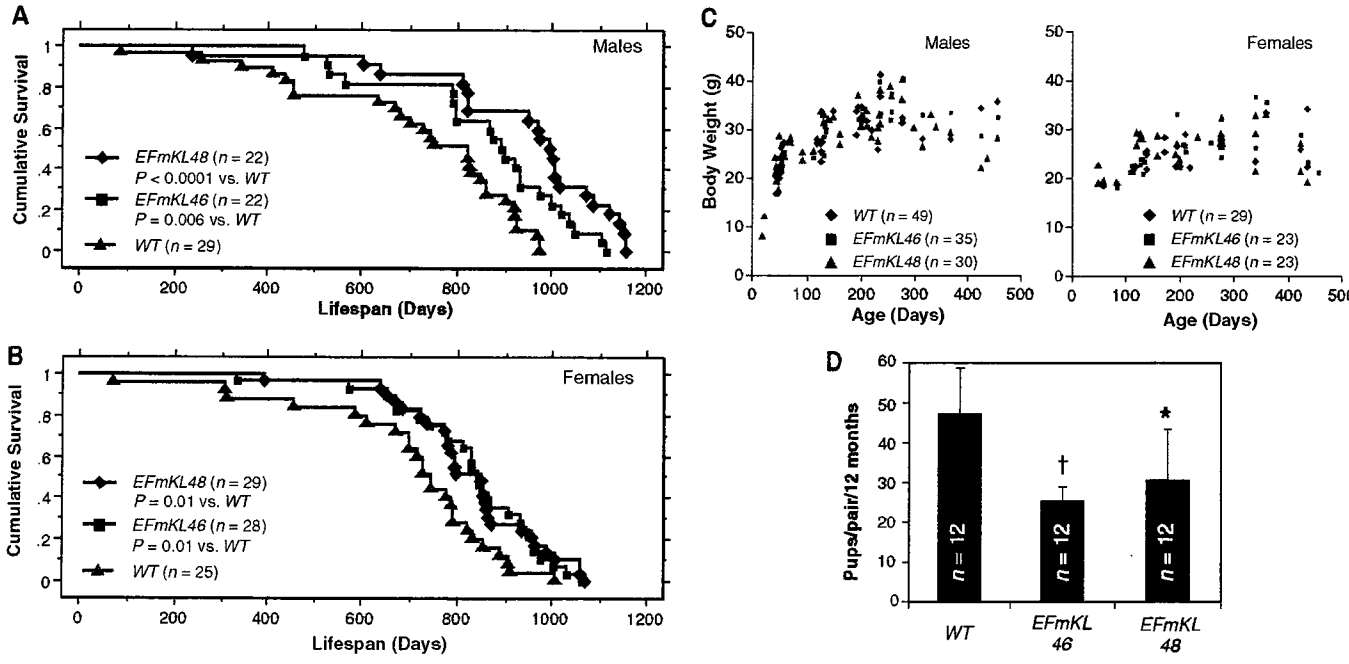

Fig. 1. Klotho overexpression extends life span in the mouse. Kaplan-Meier analysis of survival in (A) males [$P = 0.006$ in *EFmKL46* versus wild-type (WT) mice, and $P < 0.0001$ in *EFmKL48* versus wild type by log-rank test) and in (B) females ($P = 0.01$ in *EFmKL46* versus wild type, and $P = 0.01$ in *EFmKL48* versus wild type by log-rank test). The average life span of male wild-type, *EFmKL46*, and *EFmKL48* mice was 715 ± 44 days, 858 ± 40 days, and 936 ± 47 days (means ± SEM), respectively. The average life span of female wild-type, *EFmKL46*, and *EFmKL48* mice was 697 ± 45 days, 829 ± 32 days, and 830 ± 29 days, respectively. (C) Body weight of wild-type, *EFmKL46*, and *EFmKL48* mice. No significant difference in growth was observed. (D) Klotho overexpression reduces fecundity. Twelve breeding pairs at 12 weeks of age were set up for each genotype. The number of offspring generated during 12 months was recorded for each breeding pair. Although average litter size (pups per birth) of wild-type, *EFmKL46*, and *EFmKL48* pairs was not significantly different (6.6 ± 1.0, 6.1 ± 1.3, and 7.0 ± 1.2, respectively), the number of births (births per pair per 12 months) was fewer in transgenic mice pairs (7.2 ± 1.6, 4.2 ± 0.8, and 4.5 ± 2.2, respectively), resulting in significantly fewer offspring in transgenic pairs. Data are means ± SD. *, $P < 0.05$; †, $P < 0.01$ versus wild-type mice by analysis of variance (ANOVA).

degeneration, the Klotho protein may function through a circulating humoral factor that regulates the development of age-related disorders or natural aging processes (*2*). Notably, some single-nucleotide polymorphisms in the human *KLOTHO* gene are associated with altered life span (*3*) and altered risk for coronary artery disease (*4*), osteoporosis (*5–7*), and stroke (*8*).

Little is known about Klotho protein function and the molecular mechanism by which it suppresses the development of aging-like phenotypes. The extracellular domain of Klotho protein is composed of two internal repeats, KL1 and KL2, that share amino acid sequence homology to β-glucosidases of bacteria and plants (20 to 40% identity) (*1*). However, glucosidase activity is not present in recombinant Klotho protein (*9*), and the essential glutamate residue at the β-glucosidase active center is replaced with asparagine and alanine in KL1 and KL2, respectively (*10*). Here, we demonstrate that *Klotho* is an aging suppressor gene whose product functions as a hormone that inhibits intracellular insulin and IGF1 signaling.

Klotho overexpression extends life span in mice. We previously generated independent transgenic lines of mice that overexpress *Klotho* under the control of the human elongation factor 1α promoter (*1*) (*EFmKL46* and *EFmKL48*) (fig. S1). Here, we compared the life span of the transgenic mice with that of wild-type controls that are near-coisogenic by virtue of backcrossing onto the C3H background four times. Each line was previously confirmed to express functional Klotho protein from the transgene (*1*). Mice carrying the

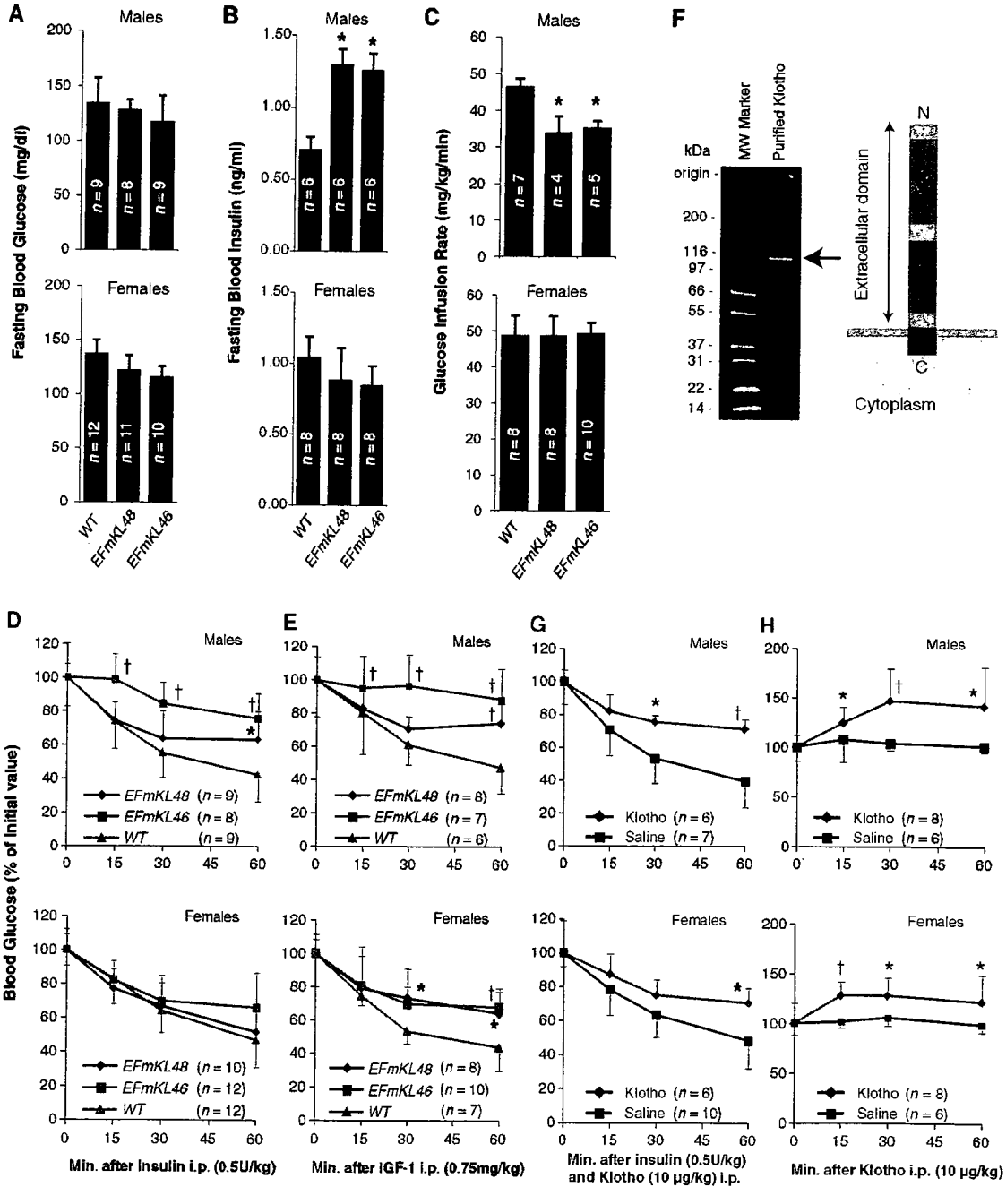

Fig. 2. Klotho increases resistance to insulin and IGF1. (**A** and **B**) Fasting blood glucose (A) and insulin (B) levels were compared between wild-type (WT), *EFmKL48*, and *EFmKL46* mice. (**C**) Hyperinsulinemic euglycemic clamp experiments. Glucose infusion rate (mg/kg/min) was compared between wild-type, *EFmKL48*, and *EFmKL46* mice. During the clamp experiments there were no differences in blood glucose concentration between wild-type, *EFmKL46*, and *EFmKL48* mice. The number of animals (*n*) for each group is indicated in the bars. (**D** and **E**) Insulin (D) and IGF1 (E) tolerance tests. Blood glucose levels after injection of insulin (0.5 U/kg) or IGF1 (0.75 mg/kg) were expressed as a percentage change from blood glucose concentration at time zero. Error bars indicate SD. *, $P < 0.05$ and †, $P < 0.01$ versus wild-type mice by ANOVA. (**F**) A schematic representation of Klotho extracellular peptide (right) and analysis of purified recombinant Klotho peptide by SDS-polyacrylamide gel electrophoresis (left). (**G**) The effect of Klotho injection on insulin tolerance in mice. Insulin tolerance tests were performed with age-matched wild-type mice immediately after intraperitoneal injection with saline or purified recombinant Klotho peptide (10 μg/kg). (**H**) The effect of Klotho injection on blood glucose levels. Saline or Klotho protein (10 μg/kg) was administered into age-matched wild-type mice by intraperitoneal injection. Error bars indicate SD. *, $P < 0.05$ and †, $P < 0.01$ versus saline-injected mice by ANOVA.

EFmKL46 or *EFmKL48* transgenic alleles, fed *ad libitum*, outlived wild-type controls by 20.0 and 30.8%, respectively, in males (Fig. 1A) and by 18.8 and 19.0%, respectively, in females (Fig. 1B).

Caloric restriction is associated with increased longevity in various species (*11*). To assess whether mice overexpressing Klotho were restricting their own diets, we monitored food intake and oxygen consumption in transgenic and wild-type mice for 24 hours at 32 to 36 weeks of age. No significant differences in these parameters were observed (table S1). Small body size is also associated with extended longevity in diet-restricted mice and in mice that are mutant for pituitary or growth hormone receptor function (*12*, *13*). However, we did not observe any substantial difference in growth between *EFmKL46*, *EFmKL48*, and wild-type mice (Fig. 1C). Both *EFmKL46* and *EFmKL48* breeding pairs generated fewer offspring than wild-type breeding pairs (Fig. 1D). As expected from the evolutionary theory of longevity, maximum fitness of the organism is a trade-off between life span and fertility (*14*). These data indicate that *Klotho* systemically modulates aging through mechanisms independent of food intake and growth, but potentially in association with reproduction.

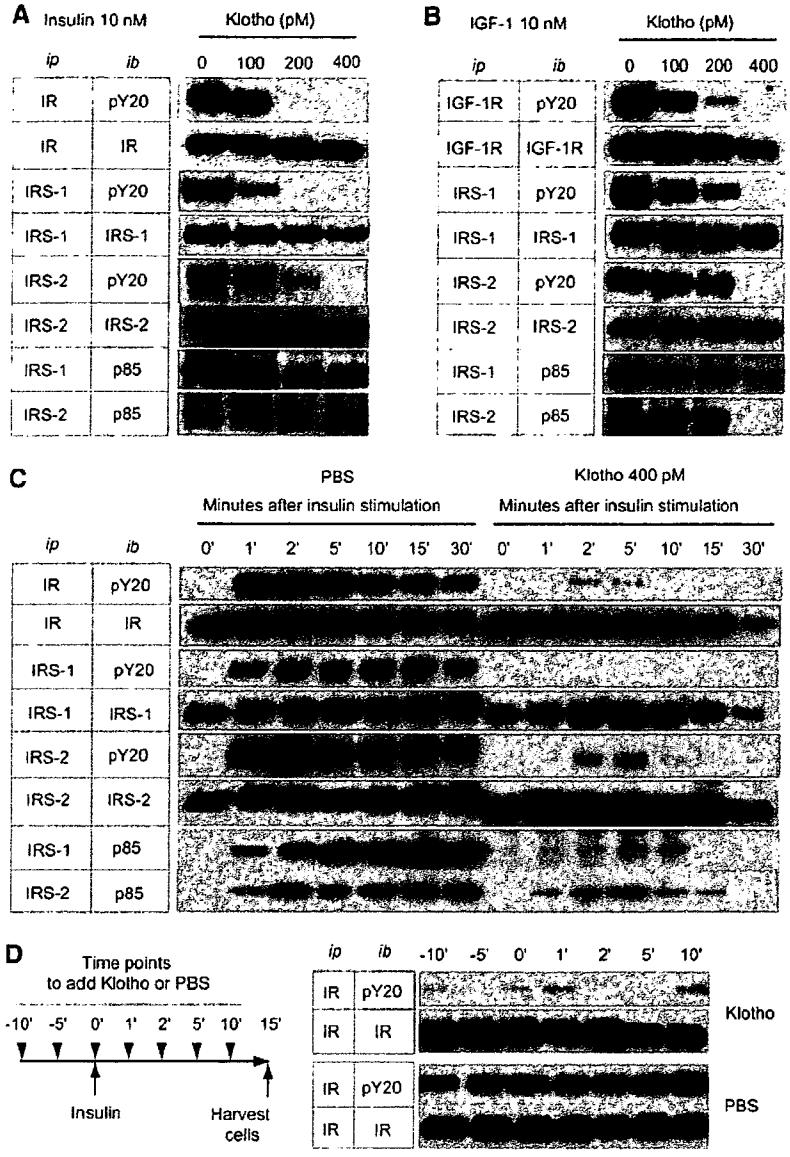

Fig. 3. Klotho protein inhibits intracellular insulin and IGF1 signaling. (**A** and **B**) Effect of Klotho on tyrosine phosphorylation of insulin and IGF1 receptors as well as IRS-1 and IRS-2, association of IRS-1 and IRS-2 with the PI3-kinase regulatory subunit (p85), and phosphorylation of Akt in L6 cells stimulated with 10 nM of insulin (A) or 10 nM of IGF1 (B). Antibodies used for immunoprecipitation (ip) and immunoblotting (ib) were indicated. IR, antibody to insulin receptor β chain; pY20, antibody to phosphotyrosine; IRS-1, antibody to IRS-1; IRS-2, antibody to IRS-2; p85, antibody to PI3-kinase regulatory subunit; IGF-1R, antibody to IGF1 receptor β chain. (**C**) A time course of the inhibitory effect of Klotho protein (400 pM) on insulin signaling in H4IIE cells. The cells were harvested before (0') and at the indicated time points after insulin stimulation (10 nM). (**D**) Inactivation of activated insulin receptor by Klotho protein. H4IIE cells were stimulated with insulin (10 nM) at time 0' and harvested 15 min later. Klotho (400 pM) or phosphate-buffered saline (PBS) was added at the indicated time points indicated (left panel). The cell lysates were immunoprecipitated with IR and immunoblotted with pY20 or IR (right panel).

Klotho increases resistance to insulin and IGF1. Many genetic data demonstrate that inhibited insulin and IGF1 signaling extends life span in animals from *C. elegans*, to *Drosophila*, to mice (*15*–*21*). Because Klotho must mediate aging through effects of a systemic hormone, we investigated whether the *Klotho* gene is involved in the inhibition of insulin or IGF1 signaling. Mice defective in *Klotho* gene expression have reduced blood glucose and insulin levels coupled with enhanced sensitivity to insulin (*22*).

We compared glucose metabolism in the Klotho-overexpressing transgenic mice with wild-type animals. Blood glucose levels were normal in each transgenic line (Fig. 2A). However, male *EFmKL46* and *EFmKL48* mice had higher blood insulin levels than did wild-type males (Fig. 2B), suggesting that the male transgenic mice are somewhat insulin resistant. We directly assessed sensitivity to insulin with a hyperinsulinemic euglycemic clamp (*23*). As expected, male *EFmKL46* and *EFmKL48* mice required lower glucose infusion rates than did wild-type males to maintain normal blood glucose levels (Fig. 2C). Furthermore, insulin and IGF1 tolerance tests revealed significant attenuation in hypoglycemic response to injected insulin and IGF1 in male transgenic mice (Fig. 2, D and E). Although we were unable to detect insulin resistance in female transgenic mice (Fig. 2, C and D), they were significantly resistant to IGF1 (Fig. 2E). These studies demonstrate that Klotho overexpression induces resistance to insulin and IGF1.

Klotho functions as a hormone. The extracellular domain of Klotho is shed on the cell surface and detected in the blood and cerebrospinal fluid in mice and humans (*24*). Immunoblot analysis of plasma with the use of rabbit anti-Klotho antiserum demonstrated that the extracellular Klotho peptide can be detected in wild-type, *EFmKL48*, and *EFmKL46* mice but not in $KL^{-/-}$ mice (fig. S2). Radioimmunoassay further demonstrated that Klotho peptide is ~100 pM in wild-type mice and about two times as high in the transgenic overexpression strains (fig. S3). The extracellular domain of Klotho may function as a hormone-like substance (*2*).

To assess the function of the Klotho extracellular peptide, we generated a soluble form of recombinant Klotho protein comprising the 952–amino acid extracellular domain, and de-